



Supporting Information

for *Adv. Sci.*, DOI: 10.1002/adv.201801423

**Multistage Delivery Nanoparticle Facilitates Efficient
CRISPR/dCas9 Activation and Tumor Growth Suppression In
Vivo**

*Qi Liu, Kai Zhao, Chun Wang, Zhanzhan Zhang, Chunxiong
Zheng, Yu Zhao, Yadan Zheng, Chaoyong Liu, Yingli An,
Linqi Shi,* Chunsheng Kang,* and Yang Liu**

Supporting Information

Multistage Delivery Nanoparticle Facilitates Efficient CRISPR/dCas9 Activation and Tumor Growth Suppression In Vivo

Qi Liu, Kai Zhao, Chun Wang, Zhanzhan Zhang, Chunxiong Zheng, Yu Zhao, Yadan Zheng, Chaoyong Liu, Yingli An, Linqi Shi, Chunsheng Kang*, Yang Liu**

Q. Liu, C. Wang, Z. Zhang, C. Zheng, Y. Zhao, Y. Zheng, Y. An, Prof. L. Shi, Prof. Y. Liu

State Key Laboratory of Medicinal Chemical Biology

Key Laboratory of Functional Polymer Materials of Ministry of Education

College of Chemistry

Nankai University

Tianjin, 300071, China

E-mail: shilinqi@nankai.edu.cn; yliu@nankai.edu.cn

K. Zhao, C. Liu, Prof. C. Kang

Tianjin Neurological Institute

Department of Neurosurgery

Tianjin Medical University General Hospital

Tianjin, 300052, China.

E-mail: kang97061@tmu.edu.cn

Table of Content

Materials	4
Synthesis of PEI-PBA.....	4
Synthesis of mPEG ₁₁₃ - <i>b</i> -PLyS ₁₀₀	5
Synthesis of mPEG ₁₁₃ - <i>b</i> -PLyS ₁₀₀ /DMMA and mPEG ₁₁₃ - <i>b</i> -PLyS ₁₀₀ /SA.....	6
Investigation on the pH-responsiveness of mPEG ₁₁₃ - <i>b</i> -PLyS ₁₀₀ /DMMA.....	6
Preparation of MDNP and SDNP	6
Electrophoresis, DLS, and TEM analysis of MDNP and SDNP	7
Evaluation of the non-specific protein adsorption and stability of MDNP	8
Fluorescence resonance energy transfer (FRET) assay	8
Cell culture.....	8
Analyses of cellular uptake and endosomal escape	9
<i>In vitro</i> gene transfection	10
Quantitative real-time PCR assay evaluating the activation of miR-524 expression	10
Western blotting analysis	11
<i>In vitro</i> cytotoxicity analysis.....	11
<i>In vivo</i> distribution of MDNP	12
Immunogenicity evaluations assessed with inflammatory cytokine secretion	13
<i>In vivo</i> tumor growth inhibition by MDNP.....	13
Detection of Pri-miR-524 expression in tumors and normal organs	14
RNA <i>in situ</i> hybridization detection of miR-524 in tumor tissues	14
Immunohistochemistry analysis and H&E staining.....	14
Statistical Analysis.....	15

Table of Figures

Figure S1. Synthesis routes of the polymers.....	16
Figure S2. ¹ H NMR spectra of the polymers.....	17
Figure S3. Cytotoxicity of the polymers.....	18
Figure S4. The capability of PEI-PBA to condense pDNA.....	19
Figure S5. Luciferase expression of PEI-PBA/pDNA transfected in LN-229 cells at different N/P ratios	20
Figure S6. Zeta potentials of PEI-PBA/pDNA polyplex, SDNP and MDNP.....	21
Figure S7. BSA adsorption of PEI-PBA/pDNA polyplex and MDNP.....	22
Figure S8. Stability of SDNP and MDNP in PBS containing 10% FBS	22
Figure S9. Endosomal escape of MDNP	23
Figure S10. <i>In vitro</i> transfection efficiency of SDNP and MDNP at different pH in LN-229 cells	24
Figure S11. <i>In vitro</i> transfection efficiency of the SDNP and MDNP in LN-229 cells	25
Figure S12. Schematic diagram of dCas9-miR-524 system.	26
Figure S13. Relative expression levels of Pri-miR-524 in cells transfected with SDNP/dCas9-miR-524.....	27
Figure S14. Plasma cytokine levels after injection of MDNP	28
Figure S15. The levels of IgE, IgM, IgG after injection of MDNP.....	29

Materials. Reagents and solvents were purchased from Sigma-Aldrich (Shanghai, china) and used as received without further purification unless otherwise noted. Dialysis membranes were purchased from Tian Nan Science and Technology (Tianjin, China). All the cell lines, including human glioma (LN-229) and human breast cancer (MDA-MB-231), were purchased from American Type Culture Collection (ATCC). The Dulbecco's Modified Eagle Medium (DMEM) growth medium, fetal bovine serum (FBS) and penicillin/streptomycin were purchased from Gibco (Thermo Fisher, USA). Linear polyethylenimine 25 kDa (PEI25K) and branched polyethylenimine 1.8 kDa (PEI1.8K) were purchased from Alfa Aesar (Shanghai, China). YOYO-1, TOTO-3, rhodamine phalloidin, LysoTracker® Green, paraformaldehyde, 4,6-diamidino-2-phenylindole dihydrochloride (DAPI), and Lipofectamine 2000 were purchased from Invitrogen (USA). Cy5-NHS and Cy3-NHS were obtained from Oukainasi Technology (Beijing, China). Bicinchoninic acid (BCA) protein assay kit was obtained from Solarbio Science & Technology (Beijing, China). Cell Counting Kit-8 (CCK-8) was obtained from Zhuangmeng Biotech (Beijing, China). Fluorescent TUNEL staining kit was obtained from Zhongshanjinqiao Biotech (Beijing, China). ABC-peroxidase, diaminobenzidine (DAB) and miRNA In Situ Hybridization (RISH) kit were purchased from Bersin Biotech (Guangzhou, China). Hairpin-it miRNA qPCR Quantitation Kit was obtained from GenePharma Biotech (Shanghai, China). All ELISA kits was purchase from Jianglai biotech (Shanghai, China). All the antibodies were purchased from Santa Cruz Biotech (Shanghai, China). EndoFree Plasmid Kit was purchased from Qiagen (USA). Luciferase reporter gene assay kit were purchased from Promega (USA). The dCas9-miR-524 plasmid DNA was constructed by Viewsolid Biotech (Beijing, China).

Synthesis of PEI-PBA. The synthesis of PEI-PBA was achieved by conjugating 2-bromomethylphenylboronic acid (PBA) onto branched polyethylenimine (PEI_{1.8K}). Briefly, 1.80 g of PEI (Mw = 1.8 kDa) was firstly dissolved in methanol to reach a concentration of

120 mg/mL, following by the addition of 0.54 g of PBA. The reaction solution was stirred under reflux at 70 °C for 12 h, and then the product was precipitated by dropping the reaction solution into cold ether. The product was dried under vacuum to achieve pale yellow solid (yield 70%). The successful conjugation was confirmed using ¹H nuclear magnetic resonance spectrum (¹H NMR). ¹H NMR (400 MHz, D₂O, δ ppm): δ=7.4-8.0: (4H, ArH), δ=2.2-3.6: (4H, -CH₂NHCH₂-).

Synthesis of mPEG₁₁₃-b-PLys₁₀₀. The mPEG₁₁₃-b-PLys₁₀₀ was synthesized by the ring-opening polymerization of Lys(Z)-NCA using MeO-PEG₁₁₃-NH₂ (Jinpan biotech, Shanghai, China) as the initiator. Briefly, Lys(Z)-NCA (5.35 g, 18.4 mmol) was dissolved in 30 ml of DMF. The polymerization was initiated by the addition of MeO-PEG₁₁₃-NH₂ (0.61 g, 0.123 mmol). The reaction mixture was stirred for 3 days at 35 °C under a dry argon atmosphere. After the reaction, the solvent was evaporated under reduced pressure. The resulting product was dissolved in 15 mL of CHCl₃ and then precipitated into excessive diethyl ether to obtain mPEG-b-PLys(Z) (yield 85%). Deprotection of Z group in mPEG₁₁₃-b-PLys(Z) was carried out by addition of HBr (33 wt.% in HOAc, 2 mL) to the solution of mPEG₁₁₃-b-PLys(Z) (2.0 g) in 20 mL CF₃COOH for 2 h at 0 °C. After precipitating using cold diethyl ether, the product was re-dissolved in DMF and filtered through a 0.22 μm Millipore filter. The filtrate was precipitated in excessive diethyl ether to remove the residual CF₃COOH and obtain mPEG₁₁₃-b-PLys (yield 65%). mPEG₁₁₃-b-PLys was characterized using ¹H NMR. As shown in Fig. S2, the degree of polymerization (DP) of Lys was estimated to be 100 by comparing the integration of the peaks of the -OCH₂CH₂- protons of PEG at 3.3-3.4 ppm and the -NHCHCO- protons of PLys at 4.2-4.4 ppm. ¹H NMR (400 MHz, D₂O, δ ppm): δ=4.2-4.4: (1H, -NHCHCO-), δ=3.6-3.8: (4H, -OCH₂CH₂-), δ=3.3-3.4: (3H, H₃CO-), δ=2.8-3.1: (2H, -CH₂CH₂CH₂CH₂NH₂), δ=1.2-1.8: (6H, -CH₂CH₂CH₂CH₂NH₂).

Synthesis of mPEG₁₁₃-b-PLys₁₀₀/DMMA and mPEG₁₁₃-b-PLys₁₀₀/SA. The synthesis of mPEG₁₁₃-b-PLys₁₀₀/DMMA was achieved by conjugating 2, 3-dimethylmaleic anhydride (DMMA) onto mPEG₁₁₃-b-PLys₁₀₀ (Fig. S1). Briefly, 100 mg of mPEG₁₁₃-b-PLys₁₀₀ was dissolved in sodium bicarbonate buffer (pH 8.5, 50 mM) to reach a concentration of 10 mg/mL, and then 211.2 mg of DMMA (five equivalents to amine groups of mPEG₁₁₃-b-PLys₁₀₀) were added. During the reaction, the pH of the solution was maintained in the range of 8.0-8.5 using 0.2 N NaOH. After the reaction, unreacted DMMA was removed by dialysis (MWCO = 3500 Da), and mPEG₁₁₃-b-PLys₁₀₀/DMMA was obtained by lyophilization.^[1] The synthesis of mPEG₁₁₃-b-PLys₁₀₀/SA was similar to that of mPEG₁₁₃-b-PLys₁₀₀/DMMA by replacing DMMA with succinic anhydride (SA). The successful synthesis was confirmed using ¹H NMR analysis (Fig. S2), indicating that approximately 90% of the amine groups on mPEG₁₁₃-b-PLys₁₀₀ reacted with DMMA or SA. ¹H NMR (400 MHz, D₂O, δ ppm): δ=4.2-4.4: (1H, -NHCHCO-), δ=3.6-3.8: (4H, -OCH₂CH₂-), δ=3.3-3.4: (3H, H₃CO-), δ=2.8-3.1: (2H, -CH₂CH₂CH₂CH₂NH₂), δ=2.2-2.5: (4H, -OCCH₂CH₂COOH) δ=2.4-2.6: (6H, -OCC(CH₃)C(CH₃)COOH), δ=1.2-1.8: (6H, -CH₂CH₂CH₂CH₂NH₂).

Investigation on the pH-responsiveness of mPEG₁₁₃-b-PLys₁₀₀/DMMA. The pH-responsiveness of mPEG₁₁₃-b-PLys₁₀₀/DMMA was studied by monitoring change of the peak of DMMA group using ¹H NMR (400 MHz, D₂O/DCl). Briefly, the mPEG₁₁₃-b-PLys₁₀₀/DMMA was dissolved in D₂O/DCl (pH=6.5) at a concentration of 1 mg/mL at 37 °C. The solution (500 μL) was immediately analyzed using ¹H NMR to access the spectra at 0 h, 0.5 h, 1 h, 1.5 h and 2 h. The shiftiness of the characteristic peak attributed to the hydrogen adjacent to amide bond/amino group (Fig. 2a) confirmed the degradation of the DMMA group of mPEG₁₁₃-b-PLys₁₀₀/DMMA in response to the acidic environment.

Preparation of MDNP and SDNP. MDNP and SDNP were prepared by mixing the solution of PEI-PBA/pDNA polyplex with mPEG₁₁₃-b-PLys₁₀₀/DMMA solution and mPEG₁₁₃-b-

PLys₁₀₀/SA solution, respectively. PEI-PBA (0.1 mL, 1.5 mg/mL in water) and dCas9-miR-524 pDNA (0.1 mL, 250 µg/mL in water) were mixed gently and incubated for 15 min to form the PEI-PBA/pDNA polyplex. To prepare MDNP, 0.1 mL of mPEG₁₁₃-b-PLys₁₀₀/DMMA solution (3 mg/mL) was added into the solution of PEI-PBA/pDNA polyplex (0.1 mL) and incubated for 15 min at room temperature. The preparation of SDNP was achieved in a similar method by employing mPEG₁₁₃-b-PLys₁₀₀/SA (0.1 mL, 3 mg/mL) instead of mPEG₁₁₃-b-PLys₁₀₀/DMMA.

Electrophoresis, DLS, and TEM analysis of MDNP and SDNP. The agarose gel retardation assay was carried out in 0.7% (w/w) agarose gel in 1×TAE buffer at a constant voltage of 120 V for 30 min. After the electrophoresis, the gel was stained with the 0.5 mg/mL ethidium bromide solution for 30 min. The plasmid DNA bands were visualized at 365 nm using a UV gel image system (SIM135A, SIMON). DNA ladder and free plasmid DNA were used as a control.

The average sizes and zeta potentials of MDNP and SDNP were determined using dynamic light scattering (DLS) measurements. The DLS measurements were performed on a laser light scattering spectrometer (BI-200SM) equipped with a digital correlator (BI-9000AT) at 636 nm at 37 °C.

The morphology of PEI-PBA/pDNA polyplex and MDNP were observed by using transmission electron microscopy (TEM, FEI Talos F200C electron microscope). For the preparation of TEM samples, PEI-PBA/pDNA polyplex and MDNP were prepared as the solutions with pH 7.4 and the concentration of pDNA at 10 µg/mL. TEM samples were prepared by drop-coating of 2 µL PEI-PBA/pDNA polyplex and MDNP onto carbon-coated copper grids (Beijing Zhongjingkeyi Technology Co., Ltd, China). Droplets of samples were contacted with the grids for 5~10 minutes, then excess amount of samples was removed. The grid was then rinsed and stained with 1% sodium uranyl acetate (5~10 µL) for 90 seconds.

Evaluation of the non-specific protein adsorption and stability of MDNP. The non-specific adsorption of MDNP was analysed using the following method. Briefly, PBS (100 μ L, 10 mM), PEI-PBA/pDNA polyplex (10 μ g pDNA, 100 μ L), and MDNP (10 μ g pDNA, 100 μ L) were mixed with 100 μ L of bovine serum albumin (BSA) solution (2 mg/mL) and incubated at 37 $^{\circ}$ C for 120 min. After the incubation, all the solutions were filtered and washed 5 times with PBS (10 mM) with centrifugal filtration (MWCO = 300 kDa) to remove unabsorbed BSA. The effluent liquid was collected and tuned to 1 mL, following by measuring the BSA concentration of each sample using BCA assay. The adsorption of BSA on nanoparticles were calculated according to the following equation:

$$\text{Adsorption (\%)} = \frac{\text{adsorbed BSA in the mixture}}{\text{BSA content in the initial sample}} \times 100$$

The stability of SDNP and MDNP in PBS containing 10% FBS was examined in phosphate buffered saline (PBS, pH 7.4, 0.01 M) with 10% FBS at 37 $^{\circ}$ C, and the size of nanoparticles was characterized at various incubation times using dynamic light scattering (DLS) measurements. The DLS measurements were performed on a laser light scattering spectrometer (BI-200SM) equipped with a digital correlator (BI-9000AT) at 636 nm at 37 $^{\circ}$ C.

Fluorescence resonance energy transfer (FRET) assay. The acidic responsiveness of MDNP and SDNP was investigated via FRET analysis. Briefly, PEI-PBA and mPEG₁₁₃-b-PLys₁₀₀/DMMA or mPEG₁₁₃-b-PLys₁₀₀/SA was labelled with Cy3 and Cy5 to yield Cy3-PEI-PBA, Cy5-mPEG₁₁₃-b-PLys₁₀₀/DMMA, and Cy5-mPEG₁₁₃-b-PLys₁₀₀/SA according to the manufacturer's instruction. PEI-PBA/pDNA polyplex, MDNP and SDNP were prepared using the fluorescence-labeled polymers. PEI-PBA/pDNA polyplex, MDNP and SDNP were dispersed in PBS (pH=7.4, 10 mM) with the same pDNA concentration (10 μ g/mL), and then measured fluorescent emission spectra at the excitation wavelength of 515 nm. As a comparison, MDNP and SDNP were also dispersed in PBS (pH=6.5, 10 mM) with the same

pDNA concentration (10 µg/mL) and incubated for 2 h. The pH was re-adjusted to 7.4 after the incubation, and the fluorescence spectra of these solutions were collected in the same method.

Cell culture. LN-229 and MDA-MB-231 were maintained in DMEM supplemented with 10% (v/v) heat-inactivated fetal bovine serum (FBS), 100 units mL⁻¹ penicillin, and 100 µg mL⁻¹ streptomycin. All cell cultures were maintained in 5% CO₂ humidified environment at 37 °C.

Analyses of cellular uptake and endosomal escape. Cellular uptake of MDNP was studied using confocal laser scanning microscope (CLSM, Olympus, FV1000) and flow cytometry (Guava, easyCyte 8HT). Briefly, MDA-MB-231 cells were seeded at a density of 1×10⁴ cells per well in a 35 mm confocal dish (Φ =15 mm) and incubated overnight for cell attachment. The cells were then exposed to MDNP and SDNP containing 1 µg YOYO-1 labeled pDNA respectively, and then incubated in complete culture medium at different pH (pH 7.4 and pH 6.5, respectively) for 2 h. After the incubation, the cells were rinsed with ice-cold PBS and fixed with fresh 4% paraformaldehyde for 15 min at room temperature. The cells were further counterstained with DAPI for cell nucleus and rhodamine phalloidin for F-actin following the manufacturer's instructions. After the staining, the cells were observed using CLSM (Olympus, FV1000). The cellular uptake efficiency of MDNP and SDNP was also assessed using flow cytometry analysis. Briefly, MDA-MB-231 cells were seeded into 6-well plates at a density of 1×10⁵ cells per well. After the overnight growth, cells were exposed to various nanoparticles containing 3 µg YOYO-1 labeled pDNA and incubated in complete culture medium at different pH (pH 7.4 and pH 6.5, respectively) for 2 h. After the trypsin digestion and centrifugation, the cells were collected, washed with cold PBS and fixed with fresh 4% paraformaldehyde for the flow cytometry analysis (Guava, easyCyte 8HT). All of these experiments were performed in triplicate.

The endosomal escape capacity of MDNP was evaluated by analyzing the colocalization of the endosomes/lysosome and pDNA after internalizing into cell. Briefly, MDA-MB-231 cells were seeded at a density of 1×10^4 cells per well in 35 mm confocal dish ($\Phi = 15$ mm) and incubated overnight for cell attachment. The cells were then incubated with MDNP containing 1 μ g TOTO-3 labeled pDNA in complete culture medium at pH 6.5. At 1, 2 and 4 h post the exposure of MDNP, the cells were stained with LysoTracker Green according to the manufacture's instruction. After the endosome/lysosome staining, the cells were washed twice with ice-cold PBS and fixed with fresh 4% paraformaldehyde for 15 min at room temperature, and then counterstained with DAPI for the easy observation of the cell nucleus. All the cells were observed using a CLSM (Olympus, FV1000).

In vitro gene transfection. To evaluate the transfection efficiency of the MDNP and SDNP at different pH, the pDNA encoding tdTomato fluorescent protein and the pDNA encoding luciferase protein were employed as reporter genes for the gene transfection studies. Briefly, cells were seeded into 24-well plates at 2×10^4 cells per well and incubated overnight in 0.5 mL DMEM with 10% FBS (v/v). Before the transfection, the culture medium was replaced with the fresh one (containing 0 or 10% serum based on the purpose) and adjusted to either pH 7.4 or 6.8. 50 μ L of MDNP, SDNP and other comparative samples were added into the cell cultures with 1 μ g pDNA/well, respectively. After 4 h incubation, the culture medium was replaced with 0.5 mL fresh medium containing 10% FBS (v/v) for further 48 h incubation. PEI_{25K}/pDNA polyplex was employed as positive controls to perform the same studies. At the end of experiment, the cells were rinsed with PBS. The luciferase activity was evaluated using Luciferase Assay Kit and normalized with the amount of proteins (RLU/ mg protein) in the lysates determined by BCA assay. The tdTomato fluorescent protein expression was observed by fluorescence microscope (CX41, Olympus) and quantified by

flow cytometry (easyCyte 8HT, guava). All of these transfection studies were performed in triplicate.

Quantitative real-time PCR assay evaluating the activation of miR-524 expression *in vitro*. Quantitative real-time PCR (qRT-PCR) was used to detect the Pri-miR-524 expression activated by MDNP/dCas9-miR-524. Briefly, MDA-MB-231 and LN-229 cells were seeded into 6-well plates at a density of 2×10^5 cells/well and incubated overnight in DMEM with 10% FBS (v/v). The culture medium was replaced and adjusted to either pH 7.4 or 6.8, following by the addition of 100 μ L of MDNP/dCas9-miR-524, SDNP/dCas9-miR-524, MDNP/NC, PEI25K/dCas9-miR-524, respectively (3 μ g pDNA/well). After 4 h incubation, the culture medium was replaced with 2 mL fresh medium containing 10% FBS (v/v) and incubated for another 48 h. After the incubation, the total RNA was extracted from the cells using TRIzol reagent (Invitrogen, USA) according to the manufacturer's instructions. A stem-loop-specific primer (GenePharma, Shanghai, China) was used to measure the expression levels of Pri-miR-524. Expression of U6 was used as an endogenous control. The miRNA was converted to cDNA using the PrimeScript RT reagent kit (TaKaRa, Tokyo, Japan) according to the manufacturer's protocol. cDNAs were quantified by SYBR PremixExTaq (TaKaRa, Japan) by DNA Engine Opticon 2 Two-Color Real-Time PCR Detection System (Bio-Rad, USA). Fold changes for the expression levels of Pri-miR-524 were calculated using the comparative cycle threshold (CT) method ($2^{-\Delta\Delta CT}$).

Western blotting analysis. Western bolt was employed to measure the protein expression levels of Smad2, Hes1 and Tead1. Briefly, MDA-MB-231 and LN-229 cells were seeded into 6-well plates at a density of 1×10^5 cells/well and then treated as the previous description. After the transfection, each group of cells was washed with PBS for three times and then solubilized in 1% Nonidet P-40 lysis buffer. Homogenates were clarified by centrifugation at 20000g for 15 min at 4 °C, and protein concentrations were determined with a BCA assay.

Total protein lysates were separated by SDS-PAGE on 10% SDS acrylamide gels, which was then transferred to PVDF membranes (Millipore, USA). The membranes were incubated with primary antibodies against Hes1, Tead1 and Smad2 (1:1000 dilution; Santa Cruz Biotechnology, Santa Cruz, CA, USA) overnight, followed by incubating with an HRP-conjugated secondary antibody (1:1000 dilution; Zhongshan Bio Corp, Beijing, China) for 1 h. GAPDH (1:1000 dilution; Santa Cruz Biotechnology) was set as a loading control.

In vitro cytotoxicity analysis. The cytotoxicity of PEI-PBA, mPEG₁₁₃-b-PLys₁₀₀/DMMA and mPEG₁₁₃-b-PLys₁₀₀/SA were determined using CCK-8 viability assay. Briefly, cells (MDA-MB-231 and LN-229) were seeded in 96-well plates at 5×10^3 cells per well and grown to 70-80% confluence, followed by replacing the culture medium with the fresh ones containing different polymers at varied concentrations (Fig. S3) for further 24 h incubation. CCK-8 was mixed with DMEM at a volume ratio of 1/9 (freshly prepared) to achieve the CCK-8 working solution. After the incubation, the cells were rinsed using PBS buffer, followed by the addition of 100 μ L CCK-8 working solution mixture and another 2 h of incubation. Quantification of the cell viability was achieved by measuring the absorbance with Tecan's Infinite M200 microplate reader ($\lambda = 450$ nm). The cell viability was calculated by referring to that of the cells without any treatment.

The in vitro anti-tumor effect of MDNP/dCas9-miR-524 were also evaluated by CCK-8 viability assay in a similar method. Briefly, MDA-MB-231 and LN-229 cells were seeded into 96-well plates at a density of 5×10^3 cells/well and incubated overnight in DMEM with 10% FBS (v/v). The cultures were adjusted to either pH 7.4 or 6.8, and then added 10 μ L of MDNP/dCas9-miR524, SDNP/dCas9-miR-524, MDNP/NC, PEI25K/dCas9-miR-524, respectively (200 ng pDNA/well). After 4 h incubation, the culture medium was refreshed and further incubated for 24 h, 48 h and 72 h. After the incubation, the cells were rinsed using PBS, and the viability was accessed using CCK-8 assay.

In vivo distribution of MDNP. To investigate on the tumor accumulating ability of MDNP, female BALB/c nude mice at 4-week old were purchased from the animal center of the Cancer Institute of Chinese Academy of Medical Science, and were bred at Compare Medicine Center, Tianjin Medical University. All experimental protocols were conducted within Tianjin Medical University guidelines for animal research and were approved by Institutional Animal Care and Use Committee. The tumor-bearing mice were established by subcutaneous injection of MDA-MB-231 cells (5×10^6 for each mouse) in the mammary fat pad. The mice were randomly divided into three groups. When the tumor volume was about 400 mm^3 , the mice were intravenous injected with 100 μL of PEI25K/pDNA polyplex, MDNP and SDNP containing 10 μg TOTO-3 labeled pDNA. At 1 h, 6 h and 24 h post-injection, the mice were sacrificed, and the major organs and the tumors were collected for ex vivo evaluation. Ex vivo images were taken by IVIS Lumina imaged system (Caliper Life Sciences, USA). The fluorescence images were analyzed using Living Image 3.1 (Caliper Life Sciences). To determine TOTO-3 labeled pDNA distribution in the tumor tissues, the tumor was fixed by 4% paraformaldehyde at 4 $^\circ\text{C}$ for 24 h and then treated with 30% sucrose solution (w/w) at 4 $^\circ\text{C}$ overnight. The tumor tissues were frozenly sectioned into 8 μm slices and air-dried for 30 min. After staining the nuclei with DAPI, the slices were observed using a CLSM (Olympus, FV1000).

Immunogenicity evaluations assessed with inflammatory cytokine secretion. 12 Male KunMing mice of 8-10-week-old were divided into 2 groups and respectively injected with 100 μL of PBS and MDNP/dCas9-miR-524 containing 10 μg pDNA per mouse via tail vein. The blood samples were collected from the mice 72 h after injection and stored overnight at 4 $^\circ\text{C}$ in a coagulant tube, which allows the blood to coagulate naturally. The blood samples were then centrifuged at 2000 rpm for 20 minutes, and the levels of IL-6, IFN- γ , TNF- α and NF-kB in the supernatant was assessed using a mouse IL-6, IFN- γ , TNF- α and NF-kB ELISA

kits following the protocol provided by the manufacture. The measurement was performed on a Tecan's Infinite M200 microplate reader.

In vivo tumor growth inhibition by MDNP. To investigate tumor growth inhibition with MDNP/dCas9-miR-524 *in vivo*, the tumor-bearing mice with MDA-MB-231 xenograft was established as described above. When the tumor volume was around 25 mm³ at 10 days after cell implantation, the mice were randomly divided into five groups (five mice per group) and intravenously injected with 100μL of PBS, MDNP/dCas9-NC, PEI_{25K}/dCas9-miR-524, SDNP/dCas9-miR-524 and MDNP/dCas9-miR-524 containing 10 μg plasmid DNA per mouse every three days. Tumor growth was monitored by measuring the perpendicular diameter of the tumor using calipers. The estimated volume was calculated according to the formula: tumor volume (mm³) = 0.5 × length × width².

Detection of Pri-miR-524 expression in tumors and normal organs. For analysis the *in vivo* upregulation of Pri-miR-524, the mice administrated with MDNP were sacrificed, and their tumors and other organs (e.g., heart, liver, spleen, lung, kidney) were collected, freed with liquid nitrogen and grind. The RNA was collected and analyzed by qRT-PCR as describe above.

RNA in situ hybridization detection of miR-524 in tumor tissues. In situ hybridization assay was performed on freshly frozen tissue sections. In brief, slices were washed with 1× phosphate buffered saline (PBS) containing 0.5% Triton X-100. The slices were then incubated with appropriate amount of anti-DANCR, anti-miR-524 oligodeoxy-nucleotide probes (BersinBio, Guangzhou, China) with hybridization solution containing 1% blocking solution in humid chamber at 37 °C overnight. After the incubation, the slices were washed three times for 5 min each at 42 °C with 0.1% Tween-20 in 4× sodium citrate buffer (SSC), once for 5 min in 2× SSC and once for 5 min in 1× SSC in dark. After rinsing with 1 × PBS for 5 min for three times at room temperature and staining with hematoxylin, the slices were

observed using a microscope (CX41, Olympus) for evaluating the expression level of miR-524.

Immunohistochemistry analysis and H&E staining. For immunohistochemistry (IHC) analysis and H&E staining, tumor tissues were immersed in 4% paraformaldehyde at 4 °C for 24 h, followed by incubating with 30% sucrose solution (w/w) overnight. The tissues were then embedded in OCT (optimal cutting temperature compound) before storing at -80 °C. 8 µm of tissue slices were prepared with cryosections and air dried for 30 min at 25 °C for IHC analysis. For Hes1, Tead1, and Smad2 analyzing, the fixed tumor sections were incubated with primary antibodies (1:100 dilutions) overnight at 4 °C, followed by incubating with biotin-labeled secondary antibody (1:100 dilutions) for 1 h at 37 °C. The sections were then incubated with ABC-peroxidase and diaminobenzidine (DAB), counterstained with hematoxylin, and visualized using light microscope (CX41, Olympus). For the deoxynucleotidyl transferase dUTP nick end labeling (TUNEL) apoptosis studying, the fixed tumor sections were stained using TUNEL Apoptosis Assay Kit according to the manufacturer's protocol. DAPI was used for nuclear counterstaining.

Statistical Analysis. Statistical comparisons were achieved using one-way ANOVA with Dunnett post-test with GraphPad Prism 5.0.

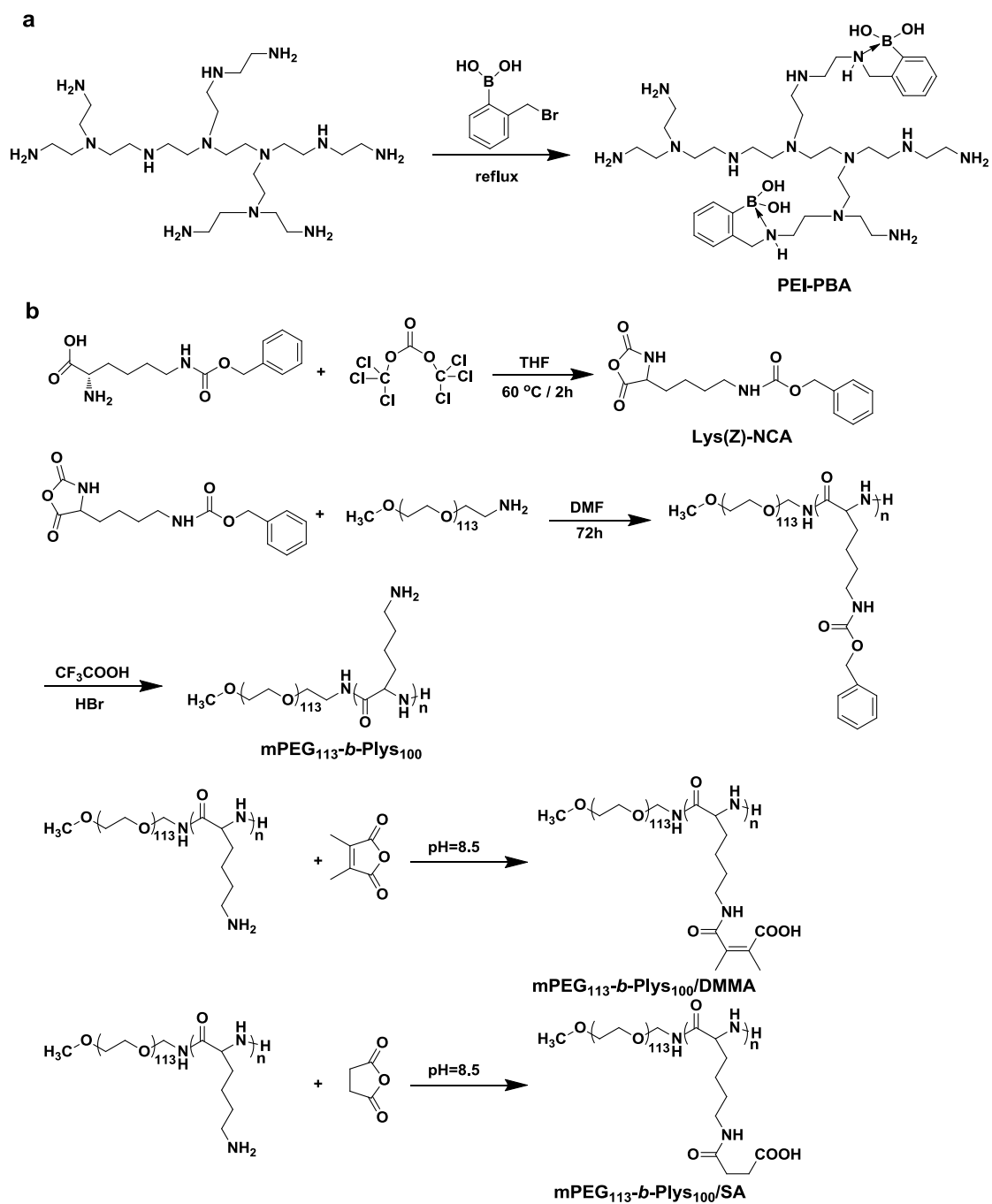


Figure S1. Synthesis routes of PEI-PBA (a), mPEG₁₁₃-b-PLys₁₀₀/DMMA and mPEG₁₁₃-b-PLys₁₀₀/SA (b).

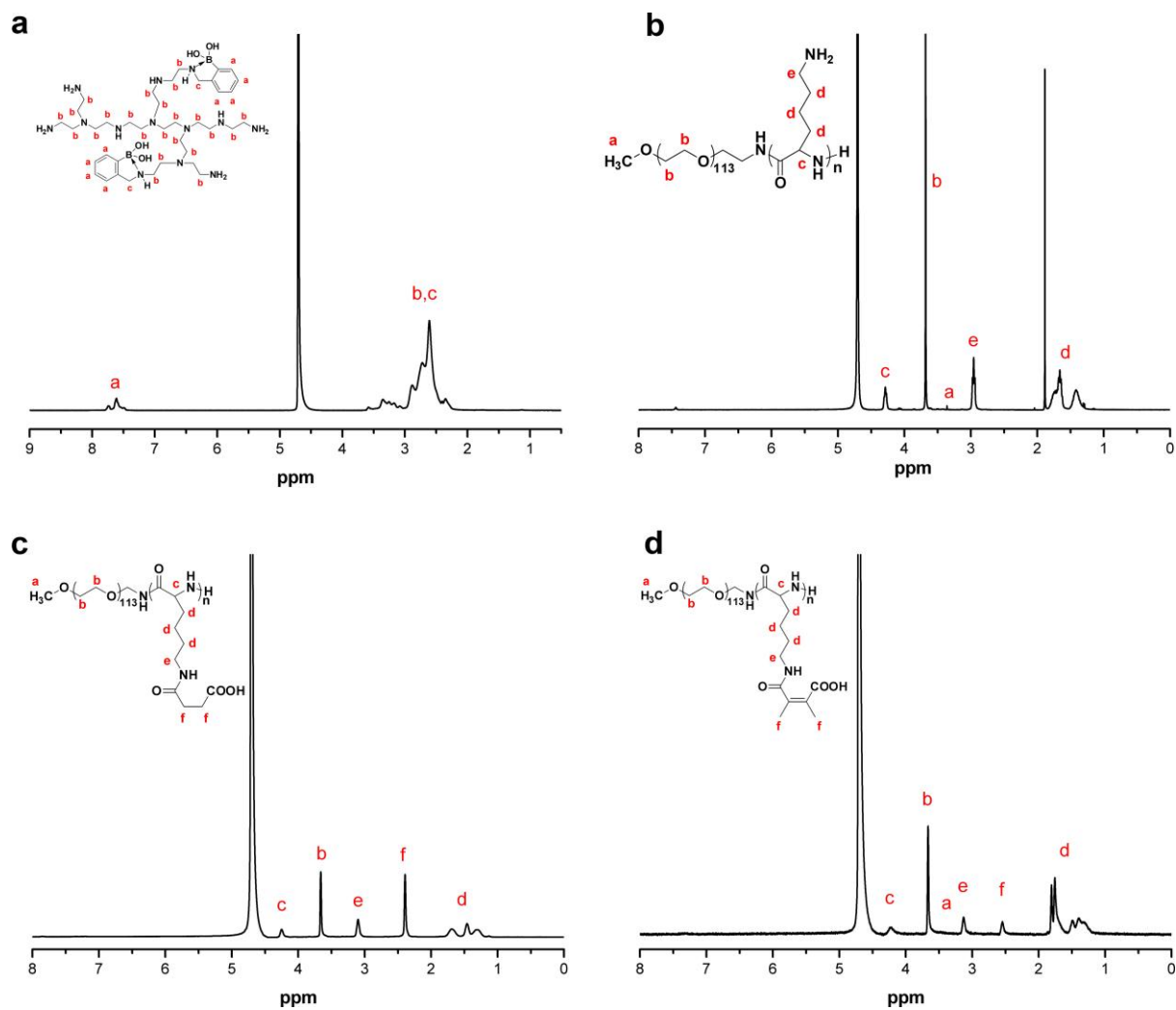


Figure S2. ^1H NMR spectra of PEI-PBA (a), mPEG₁₁₃-b-PLys₁₀₀ (b), mPEG₁₁₃-b-PLys₁₀₀/SA (c) and mPEG₁₁₃-b-PLys₁₀₀/DMMA (d) in D_2O .

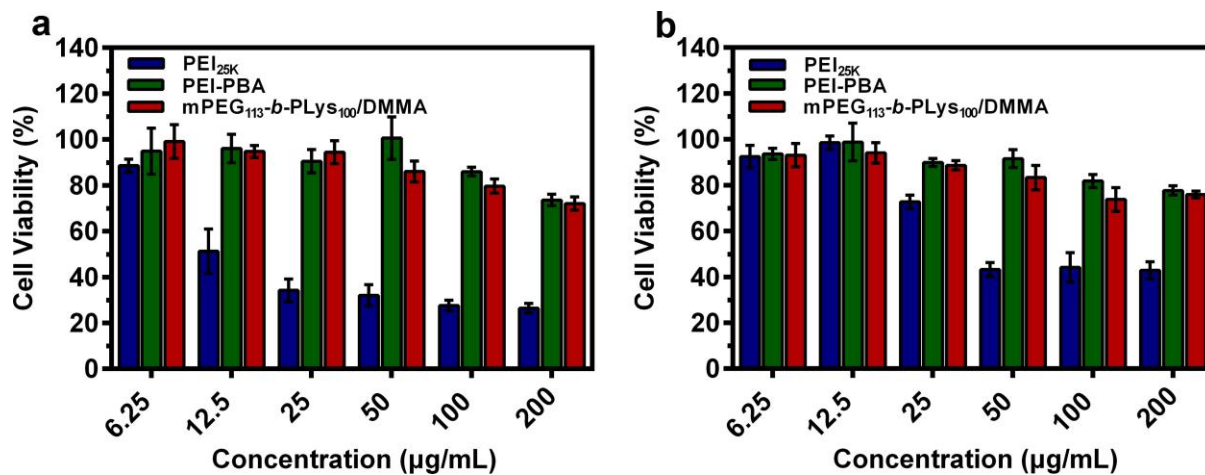


Figure S3. The cytotoxicity of PEI-PBA, mPEG₁₁₃-b-PLys₁₀₀/DMMA to LN-229 (a) and MDA-MB-231 cancer cells (b) at various concentrations. Data represent mean \pm standard deviation (s.d.) from three independent experiments (n = 3).

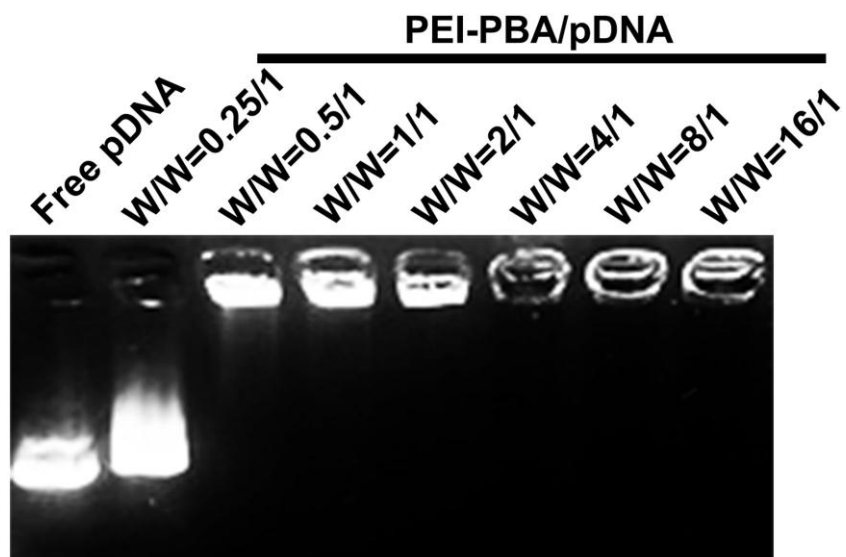


Figure S4. Gel electrophoresis presenting the capability of PEI-PBA to condense pDNA at different weight ratios. Free pDNA was used as a control.

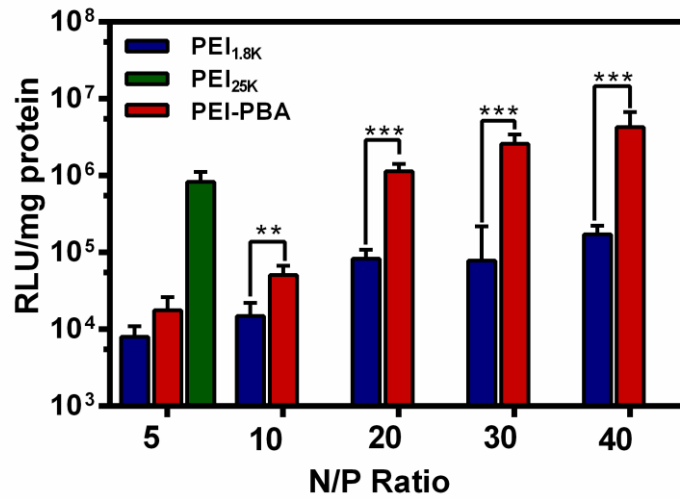


Figure S5. Luciferase expressions in LN-229 cells transfected with PEI-PBA/pDNA at different N/P ratios, PEI_{25K} and PEI_{1.8K} were used as controls. Data represent mean \pm s.d. from three independent experiments (n = 3) and the significance levels are **P<0.01, ***P<0.001.

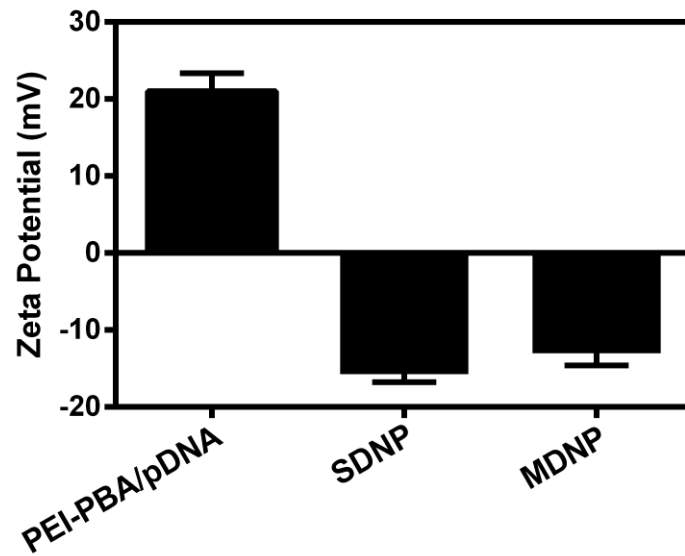


Figure S6. Zeta potentials of PEI-PBA/pDNA polyplex, SDNP and MDNP. Data represent mean \pm s.d. from three independent experiments (n = 3).

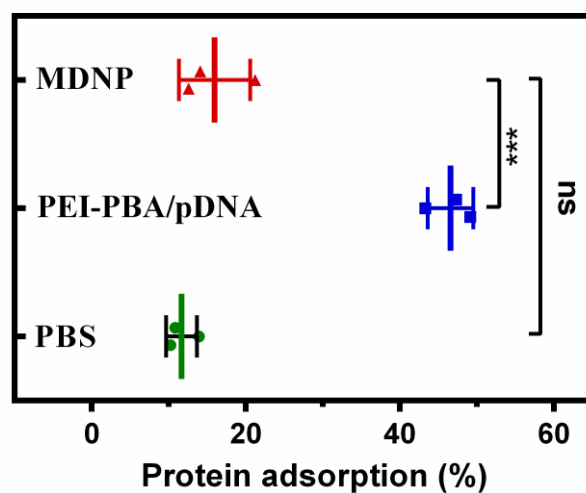


Figure S7. Quantitative measurements of BSA adsorption of PEI-PBA/pDNA polyplex and MDNP after incubation with BSA solution (1 mg/mL) for 1 h. Data represent mean \pm s.d. from three independent experiments (n = 3) and the significance levels are ***P<0.001.

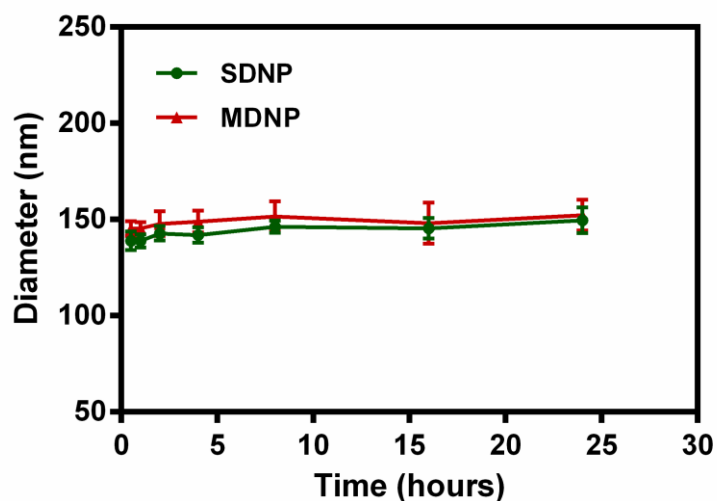


Figure S8. Stability of SDNP and MDNP in PBS containing 10% FBS.

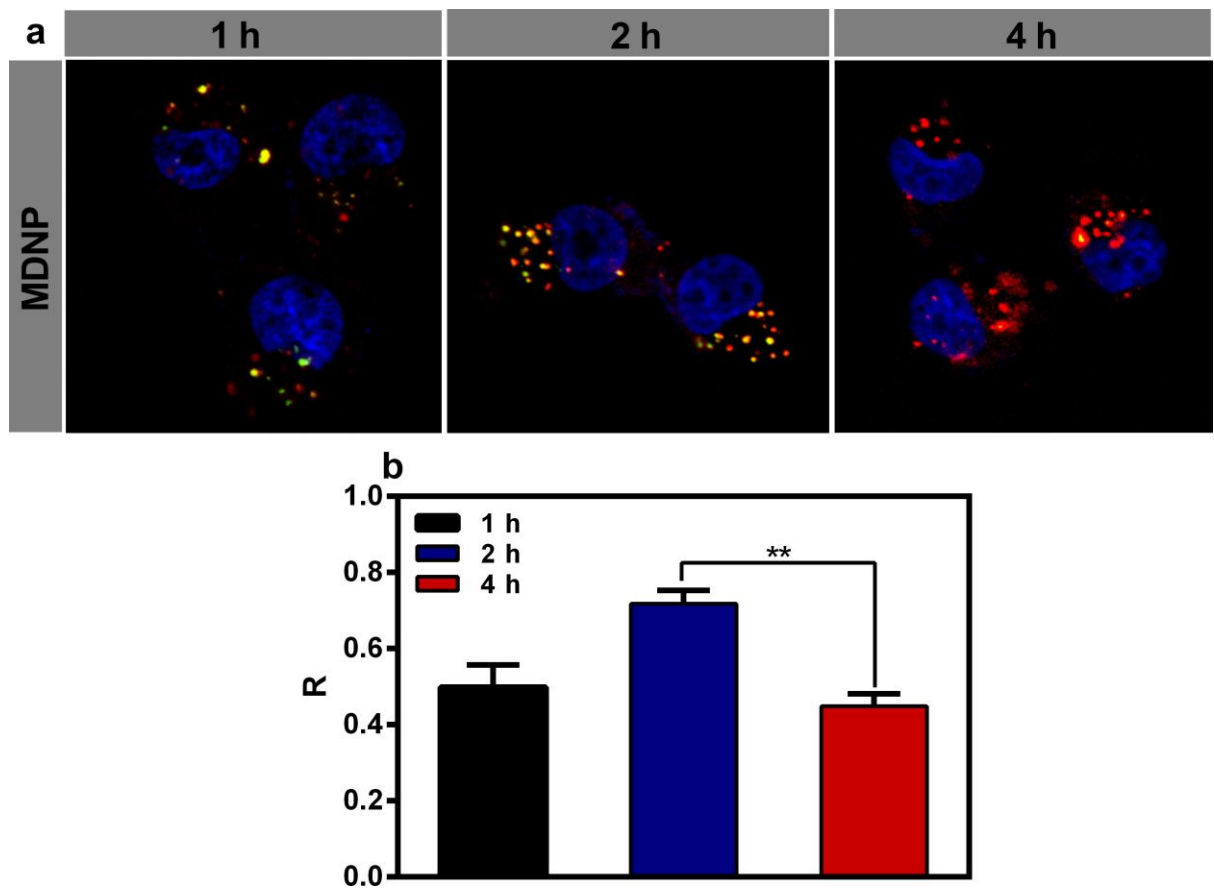


Figure S9. a) Endosomal escape of MDNP containing TOTO-3 (red) labeled pDNA. Endosomes and lysosomes were stained with LysoTracker Green, and the nuclei were stained with DAPI (blue). b) R value which represents the colocalization degree of TOTO-3 and LysoTracker Green was calculated from the CLSM images for evaluating the endosomal release efficiency. Data represent mean \pm s.d. from three independent experiments ($n = 3$) and the significance levels are $**P < 0.01$.

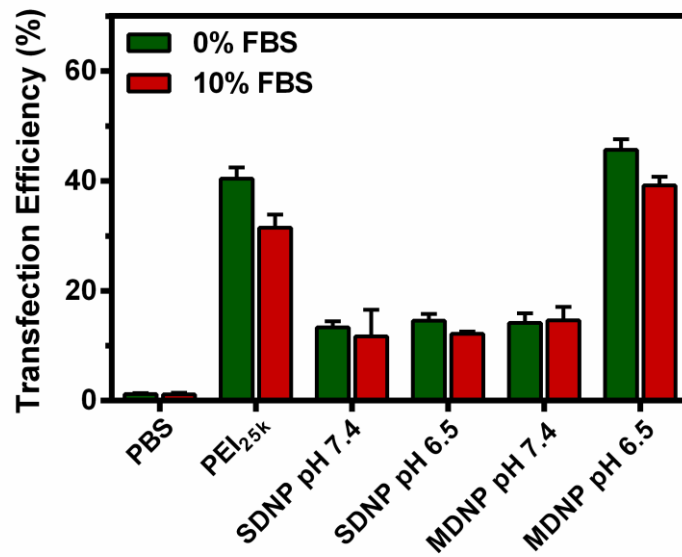


Figure S10. *In vitro* transfection efficiency of SDNP and MDNP at pH 7.4 and pH 6.5. The transfection efficiency was assessed by measuring the expression levels of tdTomato fluorescent protein in LN-229 cells using flow cytometry after the transfection. PEI_{25K} was used as the positive control. Data represent mean \pm s.d. from three independent experiments (n = 3).

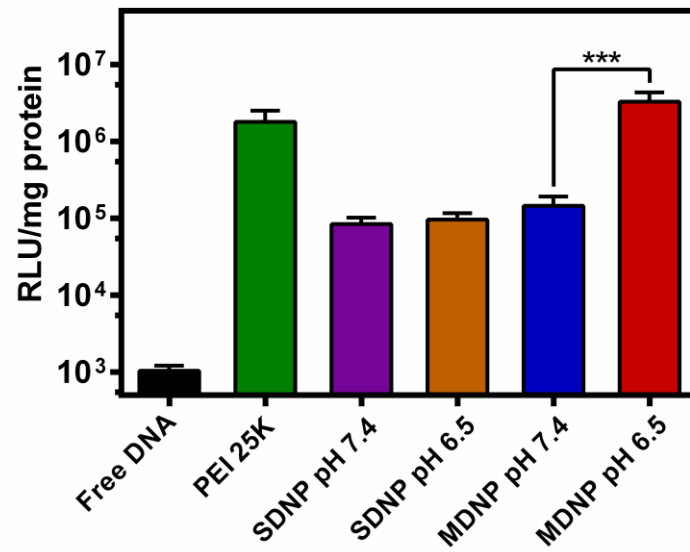


Figure S11. *In vitro* transfection efficiency of the SDNP and MDNP at pH 7.4 and 6.5. The transfection efficiency was assessed by measuring luciferase expression in LN-229 cells after the transfection. Data represent mean \pm s.d. from three independent experiments (n = 3) and the significance levels are ***P<0.001.

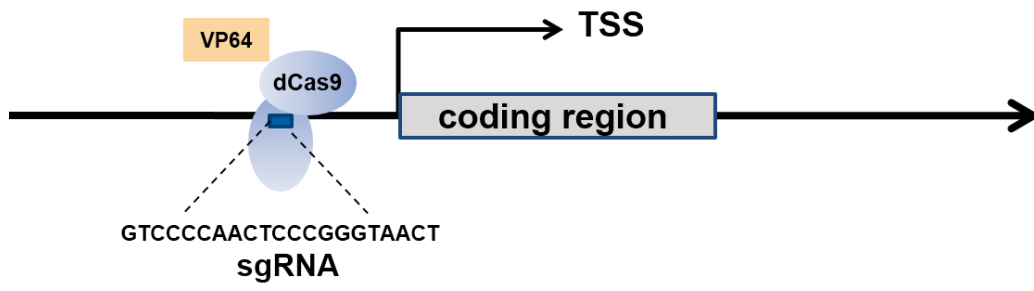


Figure S12. Schematic diagram of dCas9-miR-524 system.

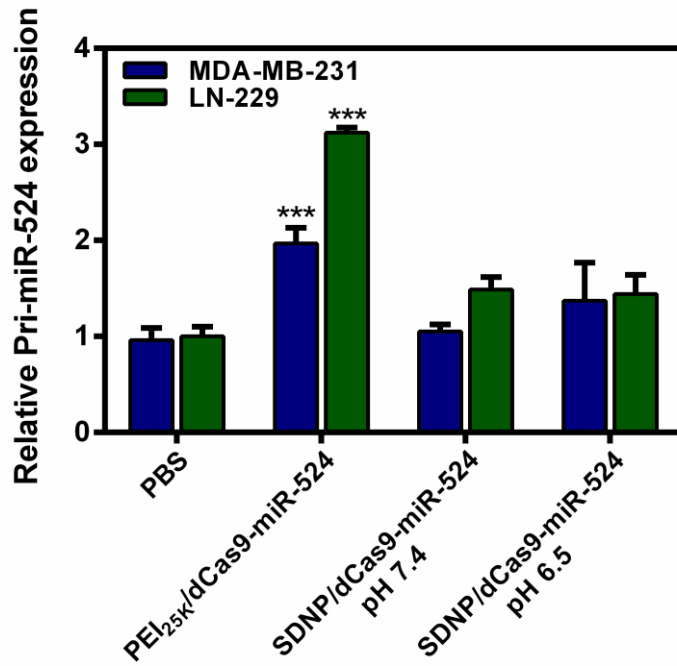


Figure S13. Relative expression level of Pri-miR-524 in LN-229 and MDA-MB-231 cells after transfecting with SDNP/dCas9-miR-524 at different pH. The expression levels of Pri-miR-524 were detected by quantitative real-time PCR assay (qRT-PCR). PEI_{25K} was employed as the positive control. Data represent mean \pm s.d. from three independent experiments (n = 3) and the significance levels are ***P<0.001.

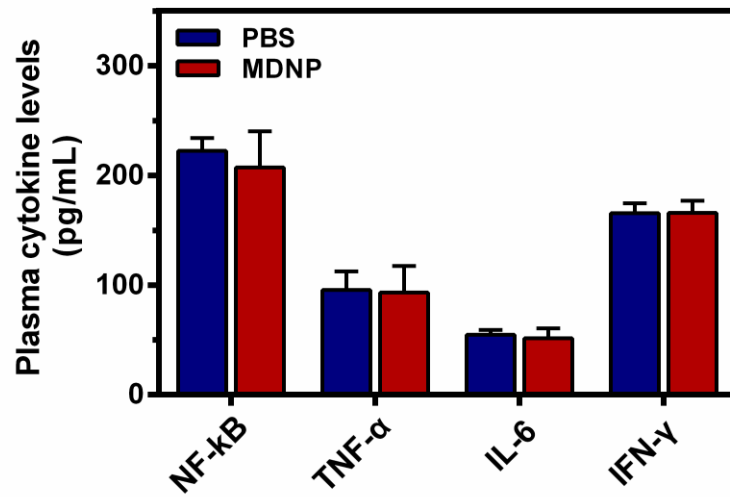


Figure S14. Plasma cytokine levels after the injection of MDNP. PBS was used as control. IFN- α , interferon α ; IL-6, interleukin 6; TNF- γ , tumor necrosis factor γ ; NF-kB, nuclear factor kB. Data represent mean \pm s.d. from six independent experiments (n = 6).

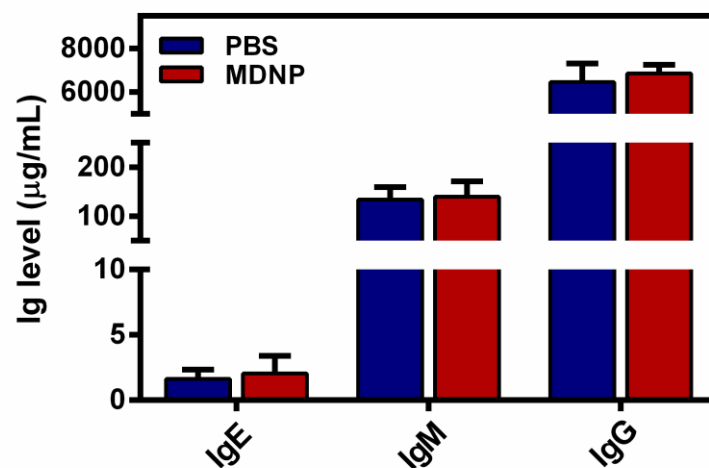


Figure S15. The levels of IgE, IgM, IgG after the injection of MDNP. PBS was used as control. Data represent mean \pm s.d. from six independent experiments ($n = 6$).

References

- [1] Y. Ding, C. Du, J. W. Qian, L. Z. Zhou, Y. Su, R. Zhang, C. M. Dong, *Polym. Chem.* **2018**, 9, 3488.

Multistage Delivery Nanoparticle Facilitates Efficient CRISPR/dCas9 Activation and Tumor Growth Suppression In Vivo

Qi Liu, Kai Zhao, Chun Wang, Zhanzhan Zhang, Chunxiong Zheng, Yu Zhao, Yadan Zheng, Chaoyong Liu, Yingli An, Linqi Shi,* Chunsheng Kang,* and Yang Liu*

CRISPR/dCas9 systems can precisely control endogenous gene expression without interrupting host genomic sequence and have provided a novel and feasible strategy for the treatment of cancers at the transcriptional level. However, development of CRISPR/dCas9-based anti-cancer therapeutics remains challenging due to the conflicting requirements for the design of the delivery system: a cationic and membrane-binding surface facilitates the tumor accumulation and cellular uptake of the CRISPR/dCas9 system, but hinders the circulating stability in vivo. Here, a multistage delivery nanoparticle (MDNP) that can achieve tumor-targeted delivery of CRISPR/dCas9 systems and restore endogenous microRNA (miRNA) expression in vivo is described. MDNP is designed as a core-shell structure in which the shell is made of a responsive polymer that endows MDNP with the capability to present different surface properties in response to its surrounding microenvironment, allowing the MDNP overcoming multiple physiological barriers and delivering the payload to tumor tissues with an optimal efficiency. Systemic administration of MDNP/dCas9-miR-524 to tumor-bearing mice achieved effective upregulation of miR-524 in tumors, leading to the simultaneous interferences of multiple signal pathways related to cancer cell proliferation and presenting remarkable tumor growth retardation, suggesting the feasibility of utilizing MDNP to achieve tumor-targeting delivery of CRISPR/dCas9 with sufficient levels to realize its therapeutic effects.


By fusing the nuclease-inactivated Cas9 (dCas9) with transcription activators and repressors, CRISPR/dCas9 system can achieve precise and efficient control of gene expression without cutting the target DNA, because the dCas9 can be directed to virtually anywhere in the genome using a short guide RNA (sgRNA).^[2] Since suppression of oncogenes or upregulation of tumor suppressor genes has been proved to be effective avenue to retard growth of tumors,^[3] therapeutics based on CRISPR/dCas9 have tremendous potential for curing cancers at transcription level.^[4] Compared to CRISPR/Cas9 systems that involve cutting and mutating the genome, CRISPR/dCas9 systems can regulate multiple oncogenic targets synergistically via modulating the transcription of endogenous microRNAs (miRNAs),^[2] providing a safer and more natural way to treat cancers.^[5] Despite several successful demonstration of applying CRISPR/dCas9 in cell line-based experiments,^[2,6] in vivo gene transcriptional regulation based on CRISPR/dCas9 for cancer therapy remains challenging due to the poor transport of CRISPR/dCas9 across multiple physiological barriers to cancer cells.

1. Introduction

Clustered regularly interspaced short palindromic repeat (CRISPR)/CRISPR-associated protein 9 (Cas9) system has emerged as a robust and versatile genome-editing platform.^[1]

The intrinsic mechanism of CRISPR system determines that it can only function inside its target cells.^[2] To this end, most of CRISPR/dCas9 studies so far have achieved the delivery via

Q. Liu, C. Wang, Z. Zhang, C. Zheng, Y. Zhao, Y. Zheng, Y. An, Prof. L. Shi, Prof. Y. Liu
State Key Laboratory of Medicinal Chemical Biology
Key Laboratory of Functional Polymer Materials of Ministry of Education
College of Chemistry
Nankai University
Tianjin 300071, China
E-mail: shilinqi@nankai.edu.cn; yliu@nankai.edu.cn

 The ORCID identification number(s) for the author(s) of this article can be found under <https://doi.org/10.1002/adv.201801423>.

© 2018 The Authors. Published by WILEY-VCH Verlag GmbH & Co. KGaA, Weinheim. This is an open access article under the terms of the Creative Commons Attribution License, which permits use, distribution and reproduction in any medium, provided the original work is properly cited.

K. Zhao, Prof. C. Liu, Prof. C. Kang
Tianjin Neurological Institute
Key Laboratory of Post-neurotrauma Neuro-repair and Regeneration
in Central Nervous System
Ministry of Education and Tianjin City
Department of Neurosurgery
Tianjin Medical University General Hospital
Tianjin 300052, China
E-mail: kang97061@tmu.edu.cn

DOI: 10.1002/adv.201801423

viral vectors.^[7] However, high immunogenicity and safety concerns limit the clinical potential of viral vector-based CRISPR gene therapies.^[8] Difficulties in the clinical translation of viral vectors empowered the investigations on synthetic vectors to accomplish such delivery.^[9] To date, several strategies based on cationic liposome,^[10] cationic polymer nanoparticles,^[10] and gold nanoparticles were successfully developed for delivery of CRISPR systems.^[11] However, all these nonviral delivery strategies have been designed and optimized for efficient CRISPR/Cas9-based gene editing in vitro and in vivo. Although some of these delivery strategies might be able to adapt to CRISPR/dCas9, a specifically designed delivery strategy for CRISPR/dCas9 is clearly anticipated to realize its full potential especially in cancer gene therapy.

From a delivery perspective, a therapeutic agent has to undergo three consecutive stages in a successful CRISPR/dCas9-based cancer treatment. Stage 1: the agent maintains stable during circulating in bloodstream, Stage 2: the agent accumulates in tumor tissues, and Stage 3: the agent enters into cancer cells, escapes from endosomes/lysosomes to cytoplasm, and enters nucleus to regulate the expression of the target gene.^[12] However, these stages require the delivery

system to have completely different surface properties, it is therefore challenging to integrate these three capabilities on a single delivery system. Herein, we present a nanoparticle-based delivery system that can achieve multistage delivery of CRISPR/dCas9 system in vivo via intravenous administration and induce the transcriptional activation of the tumor suppressor gene miR-524 in cancer cells. The multistage delivery nanoparticle (denoted as MDNP) has a core-shell structure, in which the core is a cationic polyplex made from CRISPR/dCas9 plasmid DNA (pDNA) and phenylboronic acid (PBA)-modified low molecular weight polyethyleneimine (PEI-PBA), whereas the shell is formed by 2,3-dimethylmaleic anhydride (DMMA)-modified poly(ethylene glycol)-*b*-polylysine (mPEG₁₁₃-*b*-PLys₁₀₀/DMMA) (Figure 1a). Aiming to overcome the multiple physiological barriers in the delivery of CRISPR/dCas9 system from blood to tumor cells, MDNP is designed to exhibit corresponding surface properties at different delivery stages. When circulating in bloodstream, MDNP maintains the core-shell structure. The polymer shell endows MDNP with negatively charged, PEGylated surface that effectively reduces the immune clearance.^[13] As entering tumor tissues, the acidic microenvironment induces the decomposition of

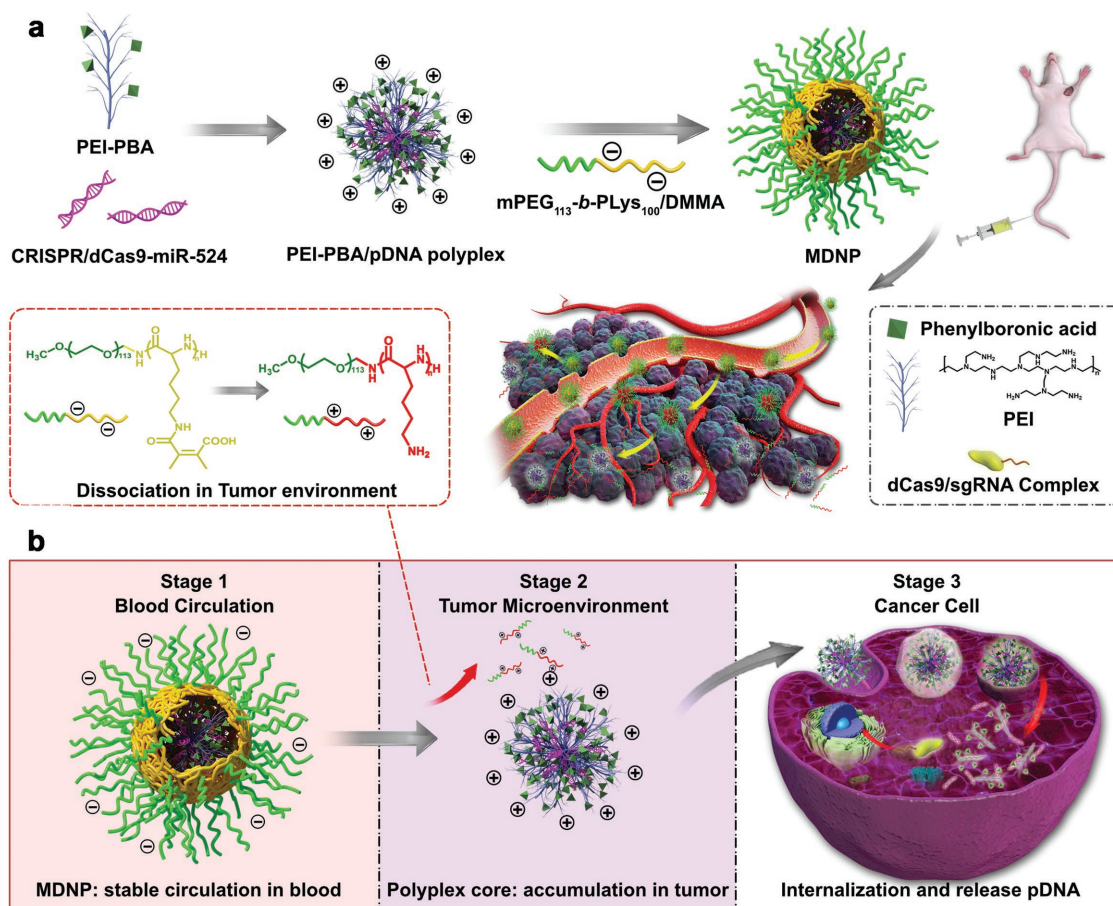


Figure 1. a) Schematic illustration for the preparation of MDNP and delivery process after intravenous injection. b) Multistage delivery of CRISPR/dCas9 system from blood circulation to tumor cells via MDNP. Stage 1: MDNP maintains stable during circulating in bloodstream. Stage 2: the dissociation of the polymer coating and exposure of the cationic core lead to the accumulation of the polyplex in tumor tissues. Stage 3: the internalization by cancer cells and the release of CRISPR/dCas9 system enable the regulation of the gene expression.

DMMA groups in the polymer shell of MDNP,^[14] leading to the rapid conversion of mPEG₁₁₃-*b*-PLys₁₀₀/DMMA from an anionic polymer to a cationic polymer (mPEG₁₁₃-*b*-PLys₁₀₀). Consequently, the polymer shell is detached from the MDNP core due to electrostatic repulsion, leading to exposure of the polyplex core with a cationic surface, which enhances the tumor accumulation and cell internalization.^[15] Moreover, since cancer cells usually have high levels of surface sialylation, the PBA groups on the polyplex can bind with those sialic acid and eventually enhance the internalization of the polyplex into cancer cells.^[16] After internalization, the PEI in the polyplex triggers the endosomal disruption and the release of CRISPR/dCas9 pDNA into the cytoplasm due to the proton sponge effect and the less entanglement between the pDNA and low molecular weight PEI–PBA,^[17] respectively (Figure 1b). With this multistage delivery strategy, MDNP achieved the efficient delivery of CRISPR/dCas9–miR-524 system and successfully inhibited the tumor growth in mice, providing a feasible approach for the development of CRISPR-based cancer gene therapeutics.

2. Results

2.1. Design, Synthesis, and Analysis of MDNP

MDNP was prepared by first constructing the CRISPR/dCas9 polyplex core via mixing PEI–PBA and CRISPR/dCas9 pDNA at a weight ratio of 6:1 (N/P ratio = 30) in a phosphate buffer saline (PBS), followed by the formation of the shell through the addition of mPEG₁₁₃-*b*-PLys₁₀₀/DMMA solution (35×10^{-9} M, pH 8.0) to reach a final weight ratio of 6:1 between the polymer and the pDNA (Figure 1a). Instead of PEI with molecular weight of 25 kDa, a PBA-modified and branched PEI (PEI–PBA) with low molecular weight ($M_w = 2081$ Da, average 2.1 PBA per PEI) was employed for the construction of the CRISPR/dCas9 polyplex for a better biocompatibility (Figure S3a,b, Supporting Information). As shown in the gel electrophoresis analysis (Figure S4, Supporting Information) and transfection efficiency tests using plasmid encoding luciferase protein as model pDNA, PEI–PBA achieved the DNA condensation successfully and exhibited acceptable transfection efficiency at N/P ratios ≥ 20 (Figure S5, Supporting Information). Dynamic light scattering (DLS) measurements revealed that the average particle size of the CRISPR/dCas9 polyplex (N/P ratio = 30) was 150.2 ± 6.9 nm, which was then confirmed with transmission electron microscopy (TEM) observation (Figure 2b). Further characterization indicated that the polyplex had a positively charged surface with zeta potential of $+22.9 \pm 5.8$ mV (Figure S6, Supporting Information), suggesting the potentials for cellular internalization and endosomal escape.

Despite the benefits for intracellular transfection of CRISPR/dCas9 plasmid DNA, the PBA-modified and positively charged surface will activate the immune clearance after administrating into bloodstream, which significantly reduces the overall delivery efficiency to tumor.^[18] To avoid the immune clearance, a layer of anionic polymer, mPEG₁₁₃-*b*-PLys₁₀₀/DMMA, was coated onto the CRISPR/dCas9 polyplex core to form MDNP with a PEGylated and negatively charged surface. The polymer

was synthesized by ring-opening polymerization of N6-carbobenzoxy-L-lysine N-carboxyanhydride (Lys(Z)-NCA) with PEG–NH₂ to achieve mPEG₁₁₃-*b*-PLys₁₀₀, followed by reacting with DMMA to achieve mPEG₁₁₃-*b*-PLys₁₀₀/DMMA (Figures S1 and S2, Supporting Information). The successful coating was confirmed with TEM and DLS measurements, leading to the increase in particle size to 205 ± 10.2 nm (Figure 2c) and the decrease in zeta potential to -12.5 ± 1.6 mV (Figure S6, Supporting Information). Moreover, coating with mPEG₁₁₃-*b*-PLys₁₀₀/DMMA reduced the nonspecific protein absorption significantly when incubating the nanoparticles with bovine serum albumin (Figure S7, Supporting Information). As a result, MDNP exhibited enhanced stability in PBS containing 10% fetal bovine serum (FBS) (Figure S8, Supporting Information), suggesting the potential to evade the immune clearance during circulation in blood.^[19]

More importantly, acidic environment (pH = 6.5) triggered the breaking of the DMMA groups apart from mPEG₁₁₃-*b*-PLys₁₀₀/DMMA, which was first confirmed by monitoring the shiftiness of the characteristic peak attributed to the hydrogen adjacent to amide bond/amino group using ¹H NMR (Figure 2a). Such conversion effectively changed the anionic polymer mPEG₁₁₃-*b*-PLys₁₀₀/DMMA into the cationic polymer mPEG₁₁₃-*b*-PLys₁₀₀, leading to the disassembly of the polymer shell from the polyplex core due to the electrostatic repulsion. For better demonstration, a nonresponsive but structurally similar polymer, mPEG₁₁₃-*b*-PLys₁₀₀/succinic anhydride (SA) (detailed structure, synthesis method, and characterizations in Figures S1 and S2 in the Supporting Information), was synthesized and coated onto the CRISPR/dCas9 polyplex core to form a comparative nanoparticle (we named it single-stage delivery nanoparticle, SDNP). The acidic responsiveness of MDNP and SDNP was then investigated via Förster resonance energy transfer (FRET) analysis. This was achieved by first labeling PEI–PBA with Cy5, and mPEG₁₁₃-*b*-PLys₁₀₀/DMMA or mPEG₁₁₃-*b*-PLys₁₀₀/SA with Cy3, and then recording the fluorescence spectra (excitation wavelength = 515 nm, Cy3) of the MDNP and SDNP made with these labeled polymers, respectively. As shown in the results, obvious FRET signals (Cy5 emission at 662 nm) were observed from both MDNP (Figure 2d, blue) and SDNP (Figure 2e, blue) at pH 7.4, indicating the successful formation of the polymer shell on the polyplex core. By changing pH to 6.5, the FRET signal from MDNP decreased significantly (Figure 2d, red), indicating the disassembly of the polymer shell. In contrast, no obvious change in FRET signal could be observed from SDNP at pH 6.5 (Figure 2e, red), suggesting that the SDNP still maintained the core–shell structure in acidic condition. Further analysis by monitoring the change in zeta potential confirmed that only MDNP presented a significant pH change from -4.8 to $+9.5$ mV of MDNP over 100 min when changing the pH to 6.5 (Figure 2f), suggesting the disassembly of the shell from MDNP and the exposure of the polyplex core. Considering the different pHs in bloodstream (pH 7.4) and tumor microenvironment (pH 6.5), this responsive shell structure allows MDNP to present different surfaces with the desired physical and chemical properties, respectively, suggesting the great potential of MDNP to overcome physiological barriers to achieve efficient delivery of CRISPR/dCas9 system to tumor cells.

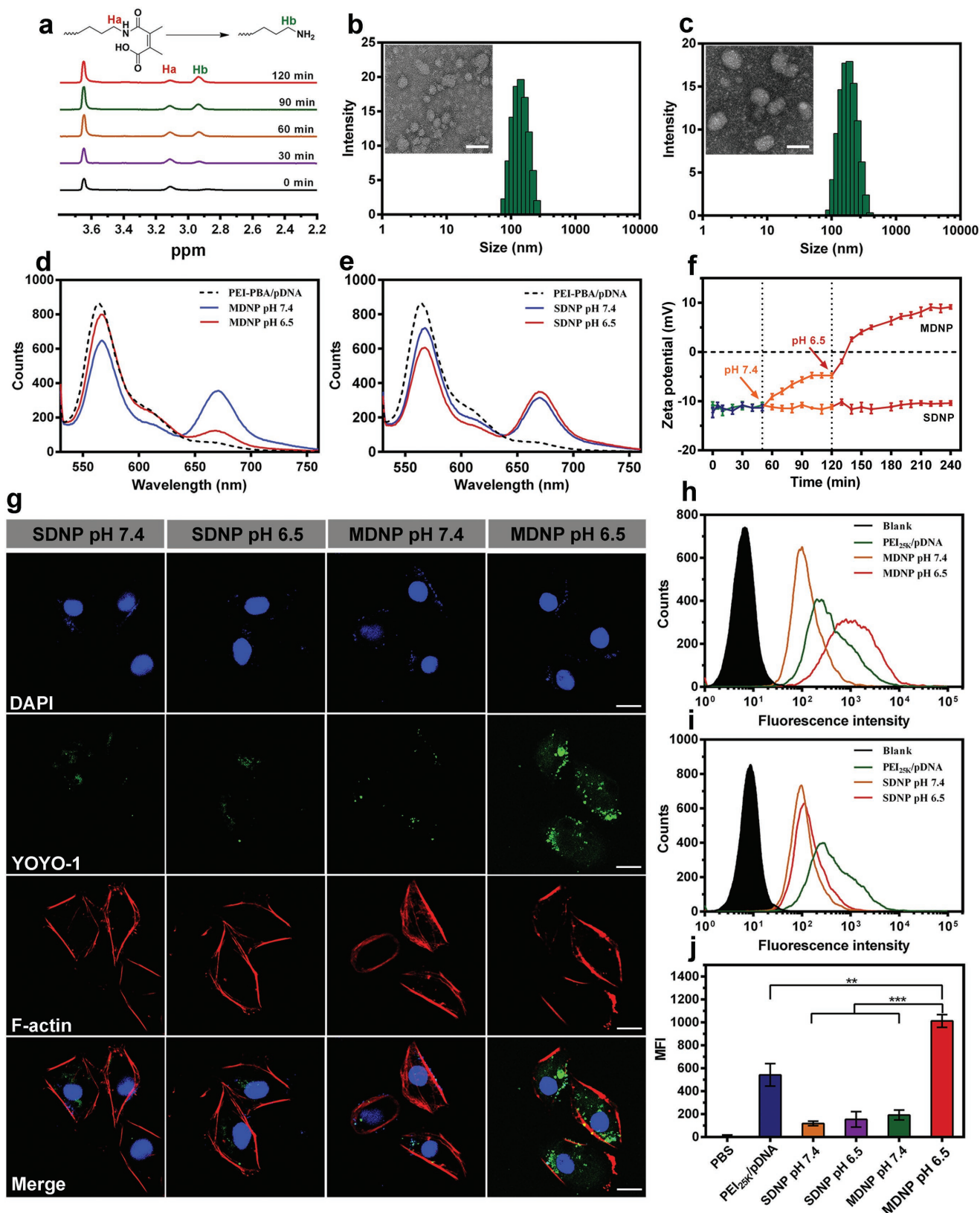


Figure 2. a) ^1H NMR spectra of $\text{mPEG}_{113}\text{-b-PLYS}_{100}/\text{DMMA}$ after being incubated at pH 6.5 in $\text{D}_2\text{O}/\text{DCI}$ (25 °C) for different time periods (Ha and Hb are attributed to the methylene protons adjacent to the amino group and amide bond, respectively). b,c) TEM images and DLS measurements of the CRISPR/dCas9 polyplex (**b**) and MDNP (**c**) (scale bar: 100 nm). d,e) Fluorescence spectra of MDNP (**d**) and SDNP (**e**) after incubated at pH 6.5 and pH 7.4. f) Zeta potential (mV) over time (min) for MDNP and SDNP at pH 6.5 and pH 7.4. g) Confocal microscopy images of cells stained with DAPI, YOYO-1, and F-actin for different polyplexes. h,i) Flow cytometry histograms for MDNP (**h**) and SDNP (**i**) at pH 6.5 and pH 7.4. j) Bar graph of Mean Fluorescence Intensity (MFI) for various polyplexes.

2.2. Cellular Internalization of MDNP and Endosomal Escape of pDNA

For an effective CRISPR/dCas9-based cancer treatment, it is crucial for MDNP to internalize into cancer cells efficiently. By preparing MDNP with YOYO-1-labeled pDNA and then incubating with cancer cells (MDA-MB-231), the cellular uptake behaviors of MDNP were observed directly with confocal laser scanning microscope (CLSM). SDNP was also employed in this study for the comparison. According to the CLSM images (Figure 2g), an obvious uptake of DNA was observed from the cells incubated with MDNP at pH 6.5. In contrast, much lower level of uptake could be observed from the cells treated with MDNP at pH 7.4, as well as those incubated with SDNP at both pHs 6.5 and 7.4. These observations were confirmed with flow cytometry analysis (Figure 2h for MDNP, and Figure 2i for SDNP). Quantitative analysis of the flow cytometry results (Figure 2j) indicated that negligible differences in uptake efficiency could be observed from the cells incubated with SDNP at different pHs, whereas a significant enhanced uptake efficiency was observed from the MDNP-treated cells when incubating at pH 6.5. This result confirmed the pH-responsive capability of MDNP, indicating that the acidic environment triggered the dissociation of the polymer shell of MDNP and the exposure of the cationic polyplex. Additional comparison with PEI_{25k}/pDNA (pH 6.5) indicated that MDNP exhibited 1.9-fold higher cellular uptake efficiency, which could be caused by the PBA groups conjugated on the surface of the polyplex.

Effective endosomal escape is another necessary step for a successful delivery of CRISPR/dCas9 system. Since the polyplex core of MDNP was made from PEI–PBA, it was expected to effectively escape from the endo-/lysosomes and release pDNA into cytoplasm due to the protonation of PEI–PBA that disrupted the endo-/lysosomes.^[20] To investigate the endosomal escape capability, MDNP carrying TOTO-3-labeled pDNA was exposed to MDA-MB-231 cells (cultured at pH 6.5), and the cells were then observed using CLSM after 1, 2, and 4 h incubation. Before the observation, the late endosomes and lysosomes of the cells were stained with LysoTracker Green. As shown in the fluorescence images (Figure S9a, Supporting Information), the colocalizations (yellow) of TOTO-3-labeled pDNA and late endo-/lysosomes were observed after 2 h incubation, indicating the entrapment of the pDNA in late endosomes and lysosomes. Following another 2 h incubation, the fluorescence signal of the pDNA (red) was clearly observed, implying the successful endosomal escape of the pDNA delivered by MDNP. Further calculation of the overlap coefficient (*R*) (Figure S9b, Supporting Information) confirmed the CLSM observation, indicating the decrease in the colocalizations of the endo-/lysosomes and the pDNA after 4 h incubation. These results

confirmed the capability of MDNP to escape from endo-/lysosomes and deliver the pDNA into the cytoplasm, allowing the effective expression of pDNA in the targeted cells.

2.3. Transfection Efficiency of MDNP in Cancer Cells

Since efficient dCas9 protein expression is a prerequisite for CRISPR/dCas9-based cancer treatment, we studied the gene transfection efficiency of MDNP in LN-229 cell line. For the easier observation, pDNA that expresses tdTomato fluorescent protein was employed for studying the transfection efficiency. As shown in Figure 3a, very low level of tdTomato expressions was observed from the SDNP-treated LN-229 cells (at pH 6.5 and pH 7.4) and the MDNP-treated cells at pH 7.4, which was caused by the inefficient cellular uptake of the nanoparticles. In contrast, high level expression of tdTomato was observed in the cells treated with MDNP at pH 6.5, and the portion of tdTomato-positive cells was higher than that of the cells treated with PEI_{25k}/pDNA, which agreed with the results from the cell uptake analysis (Figure 2j). More importantly, the introduction of 10% FBS did not impact the transfection efficiency of MDNP significantly, whereas the efficiency of PEI_{25k}/pDNA was reduced in the same condition (Figure 3a and Figure S10 (Supporting Information)). This is because the polyplex core of MDNP facilitated the transfection of pDNA using low molecular weight PEI–PBA, resulting in less nonspecific protein absorption and stronger binding to cell membrane via PBA–sialic acid complexation compared with PEI_{25k}. Further transfection studies using luciferase-expressing pDNA yielded a similar result (Figure S11, Supporting Information). With all these evidences, we can conclude that MDNP could efficiently transfect pDNA into cancer cells to express the genes of interest. Successful transfection in the presence of serum further suggests the potential of MDNP to achieve efficient gene transfection *in vivo*, which is essential for CRISPR/dCas9-based cancer gene therapy.

2.4. CRISPR Activation of miR-524 Expression with MDNP in Cancer Cells

Recent research has identified that miR-524 is usually suppressed in many types of cancer cells. Overexpression of this miRNA can restrain the proliferation and migration of cancer cells, which could potentially benefit to the overall survival of cancer patients.^[21] Upregulation of miR-524 expression using MDNP was performed on two cancer cell lines (MDA-MB-231 and LN-229) to investigate the ability of MDNP to induce CRISPR/dCas9-based gene transcriptional regulation and

7.4 for 2 h. Cy5–PEI–PBA and Cy3–mPEG₁₁₃-*b*-PLys₁₀₀/DMMA or Cy3–mPEG₁₁₃-*b*-PLys₁₀₀/SA were employed for the preparation of the MDNP and SDNP, respectively. Excitation wavelength was set at 515 nm. f) Zeta potential variation of MDNP and SDNP with the pH adjustment from pH 8.0 to pH 7.4, and then to pH 6.5. g) CLSM images of the internalization of SDNP and MDNP carrying YOYO-1-labeled pDNA (green) at different pHs after 2 h incubation with MDA-MB-231 cells. Cell cytoskeleton F-actin and cell nuclei were counterstained with rhodamine phalloidin (red) and 4,6-diamino-2-phenyl indole (DAPI) (blue), respectively. The scale bars are 20 μm. h,i) Flow cytometry analyses of the cells after incubated with SDNP (h) and MDNP (i) carrying YOYO-1-labeled pDNA at pH 7.4 and pH 6.5 for 2 h, respectively. j) Quantification of cell internalization shown by mean fluorescence intensity (MFI). Data in (f) and (j) are presented as mean ± standard deviation (s.d.) from three independent experiments (*n* = 3). The significant levels are shown as ** *p* < 0.01 and *** *p* < 0.001.

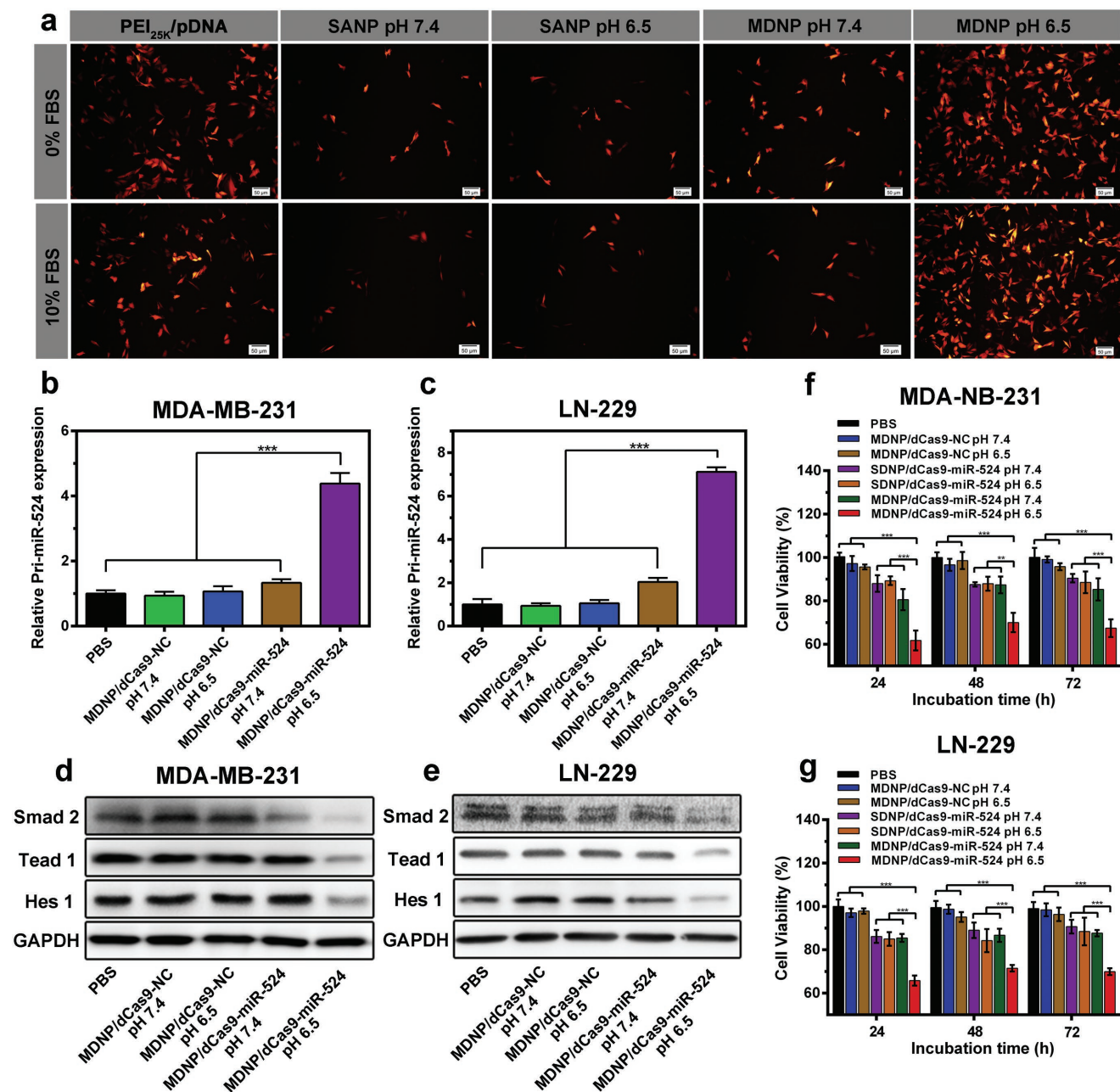


Figure 3. a) Fluorescence microscope images of LN-229 cells transfected with MDNP carrying pDNA encoding tdTomato fluorescent protein (orange) in culture media with 0% or 10% serum, respectively. The scale bar is 50 μ m. b, c) Relative expression levels of Pri-miR-524 in MDA-MB-231 (b) and LN-229 (c) cells after treating with MDNP. The expression of Pri-miR-524 was detected by quantitative real-time PCR assay. d, e) Western blot analysis of the Smad2, Tead1, and Hes1 expressions in MDA-MB-231 (d) and LN-229 (e) cells after treating with MDNP. Glyceraldehyde 3-phosphate dehydrogenase (GAPDH) was used as a loading control. f, g) Cell viability of MDA-MB-231 (f) and LN-229 (g) cells after treating with MDNP at pH 7.4 and pH 6.5 for 24, 48, and 72 h incubation. Cell viability was assessed using CCK-8 assay. All data in (b), (c), (f), and (g) are presented as mean \pm s.d. from three independent experiments ($n = 3$). The significant levels are shown as ** $p < 0.01$ and *** $p < 0.001$.

eventually suppress the proliferation of cancer cells. To this end, a pDNA (we named it dCas9-miR-524), which expresses dCas9 activator (dCas9VP64) and a sgRNA that targets the promoters or enhancers of the primary transcription content of miR-524 (Pri-miR-524), was first constructed (detailed method in Figure S12 in the Supporting Information). A nonfunctional expression vector (named NC) was also employed as the negative control for the following studies. MDNP carrying dCas9-miR-524

(MDNP/dCas9-miR-524) was incubated with the cells (MDA-MB-231 and LN-229, respectively) for 2 h. The cells were then rinsed with PBS for 3 times and for further cultured with fresh medium for 48 h. The expression level of Pri-miR-524 was analyzed via quantitative real-time polymerase chain reaction (qRT-PCR). For comparison, MDNP carrying NC (MDNP/NC) was also employed to perform the same study. According to the results (Figure 3b,c), the expression levels of Pri-miR-524

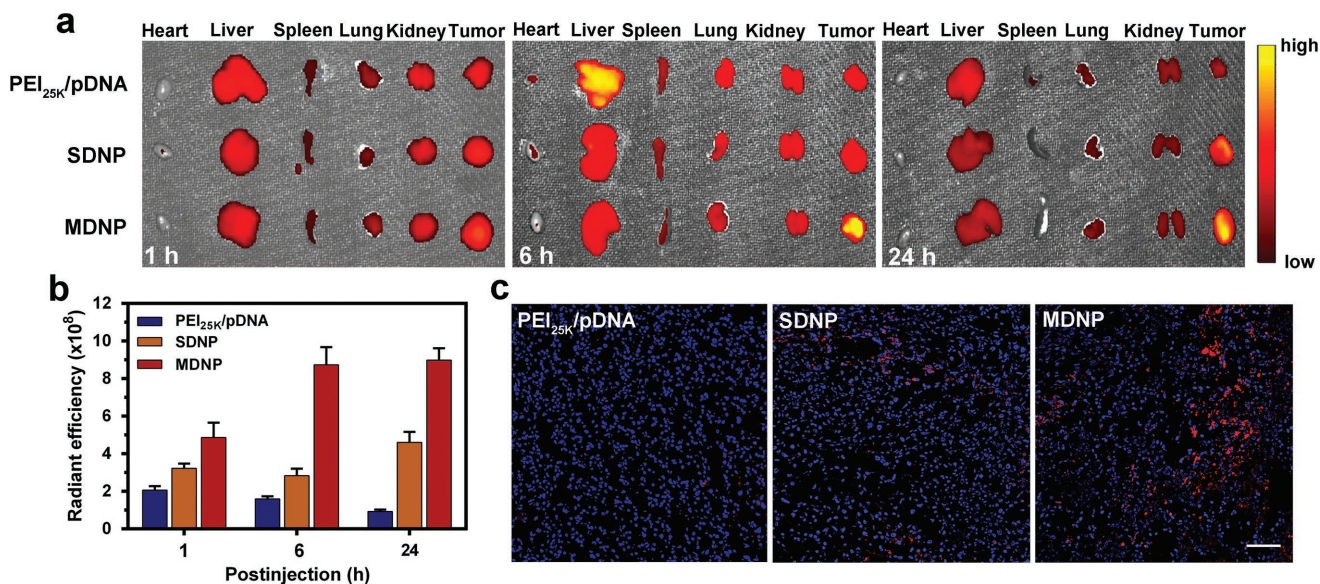


Figure 4. a) Ex vivo fluorescence images of isolated tissues from the MDA-MB-231 tumor-bearing mice after intravenous injection of PEI_{25k}/pDNA, SDNP, and MDNP carrying TOTO-3-labeled pDNA (red) at 1, 6, and 24 h postinjection. b) Quantitative analysis of the tumor accumulation of the pDNA based on the fluorescence intensity from the ex vivo images. c) CLSM images of the tumor sections from the mice 24 h postinjection. The cell nuclei were stained with DAPI (blue), and the pDNA was stained with TOTO-3 (red). The scale bar is 100 μ m. Data in (b) are presented as mean \pm s.d. from three independent experiments ($n = 3$).

were significantly upregulated to 438% in MDA-MB-231 and 711% in LN-229 when incubating with MDNP/dCas9-miR-524 at pH 6.5 (100% for untreated cells). In contrast, no significant upregulation of Pri-miR-524 expression could be observed from the cells treated with SDNP carrying dCas9-miR-524 (SDNP/dCas9-miR-524), no matter at pH 7.4 or pH 6.5 (Figure S13, Supporting Information). This result indicated that MDNP could only achieve the CRISPR activation in acidic environment, which effectively minimizes the Pri-miR-524 upregulation in tissues other than tumor and thus reduce the potential side effects.

The expression of miR-524 can restrain the proliferation of cancer cell via targeting and inhibiting the expression of Smad2, Hes1, and Tead1 which are essential proteins for transforming growth factor- β (TGF- β), Norch, and Hippo signaling pathways,^[21,22] respectively. For this reason, upregulation of endogenous miR-524 expression should decrease the expression level of these target proteins, and eventually inhibit the proliferation of the cancer cells. The expression of Smad2, Hes1, and Tead1 was accessed via Western blot analysis after treating the cancer cells with MDNP in the abovementioned conditions. As shown in Figure 3d,e, the expression levels of these three proteins were reduced significantly in the cells treated with MDNP at pH 6.5, whereas no differences in the protein expression levels could be observed from other groups compared to the untreated cells. This result is in agreement with the expression level of Pri-miR-524, which confirmed again the successful CRISPR activation mediated by MDNP. Moreover, this result also confirmed the capability of MDNP/dCas9-miR-524 to regulate multiple oncogenic pathways synergistically via the transcriptional control of endogenous miR-524, suggesting the great potential of MDNP/dCas9-miR-524 in repressing tumor growth.

To evaluate the antitumor effect of MDNP/dCas9-miR-524, cancer cells (MDA-MB-231 and LN-229) were incubated with

MDNP/dCas9-miR-524, SDNP/dCas9-miR-524, and MDNP/NC at pHs 6.5 and 7.4, respectively. The cell viabilities were then measured using cell counting kit-8 (CCK-8) after 24, 48, and 72 h incubation. Figure 3f,g summarizes the relative cell viabilities after the incubation (100% for untreated cells at 24, 48, and 72 h, respectively). Obviously, the cells incubated with MDNP/dCas9-miR-524 at pH 6.5 exhibited significant lower viability (64% at most) than any other comparative groups, suggesting the antiproliferative capacity of MDNP/dCas9-miR-524 that can be only activated in acidic environment. Moreover, negligible loss of viability was observed from the cells treated with MDNP/NC (Figure 3f,g), indicating that MDNP itself was nontoxic and thus the loss of viability of MDNP/dCas9-miR-524-treated cells was caused by the CRISPR activation of miR-524 expression.

2.5. Tumor-Targeting Capability of MDNP in Mice

For an effective CRISPR/dCas9-based cancer gene therapy, it is essential to deliver the CRISPR/dCas9 system to tumor tissue after the administration. MDNP is specially designed for the in vivo delivery of CRISPR/dCas9 system to overcome delivery barriers and accumulate in tumor tissue. To investigate on the tumor accumulating ability of MDNP, pDNA was stained with TOTO-3 and loaded into MDNP. The MDNP was then injected into tumor-bearing (MDA-MB-231) mice through tail vein. All experimental protocols were conducted within Tianjin Medical University guidelines for animal research and were approved by Institutional Animal Care and Use Committee. At different time points, the mice were sacrificed, and the major organs and the tumors were collected for ex vivo evaluation. **Figure 4a** compares the accumulation of the pDNA delivered via different systems. As shown in the ex vivo images, pDNA

delivered with PEI_{25k} failed to reach the tumor, resulting in a rapid accumulation in liver 6 h postinjection and the subsequent clearance from major organs within 24 h. In contrast, both SDNP and MDNP achieved the delivery of pDNA into tumor after the intravenous injection. Considering the nanoscaled size of SDNP and MDNP, the tumor accumulation should be caused by the enhanced permeability and retention (EPR) effects.^[23] Compared to SDNP, MDNP exhibited significantly higher level of pDNA in tumor at 6 h postinjection, suggesting a much faster accumulation. This was caused by the dissociation of the PEGylated shell and the exposure of the polyplex core of MDNP in response to the acidic tumor microenvironment. Since the polyplex core of MDNP possesses a cationic surface with PBA groups, the affinity between the nanoparticle and the tumor tissue was enhanced significantly,^[16] leading to a more efficient accumulation. Quantitative analysis of the tumor accumulation from the ex vivo images (Figure 4b) indicated that delivering via MDNP achieved a significantly higher level of pDNA in tumor compared to those delivered with SDNP and PEI_{25k} especially at 6 and 24 h postinjection. Moreover, negligible differences in the radiant efficiency of the

pDNA in tumor could be observed between 6 and 24 h when delivered using MDNP, suggesting that the exposure of the polyplex core of MDNP might further enhance the penetration and intracellular uptake of the pDNA. CLSM observation of the tumor sections (Figure 4c) indicated a remarkably higher level of pDNA throughout the tumor tissue from the mice treated with MDNP, suggesting the high delivery efficiency of MDNP in tumor-targeted delivery of pDNA.

2.6. Tumor Growth Inhibition with MDNP/dCas9–miR-524

Based on the successful tumor-targeted delivery of pDNA, additional studies were performed to investigate the potential of MDNP in CRISPR/dCas9-based cancer gene therapy. MDNP/dCas9–miR-524 was injected into tumor-bearing mice (MDA-MB-231) via tail vein every 3 days for 20 days. For better comparison, comparative groups, including PBS, MDNP/NC, PEI_{25k}/dCas9–miR-524, SDNP/dCas9–miR-524, were employed to perform the same study. A continuous monitoring of the tumor volumes during the 20 days (Figure 5a) indicated that

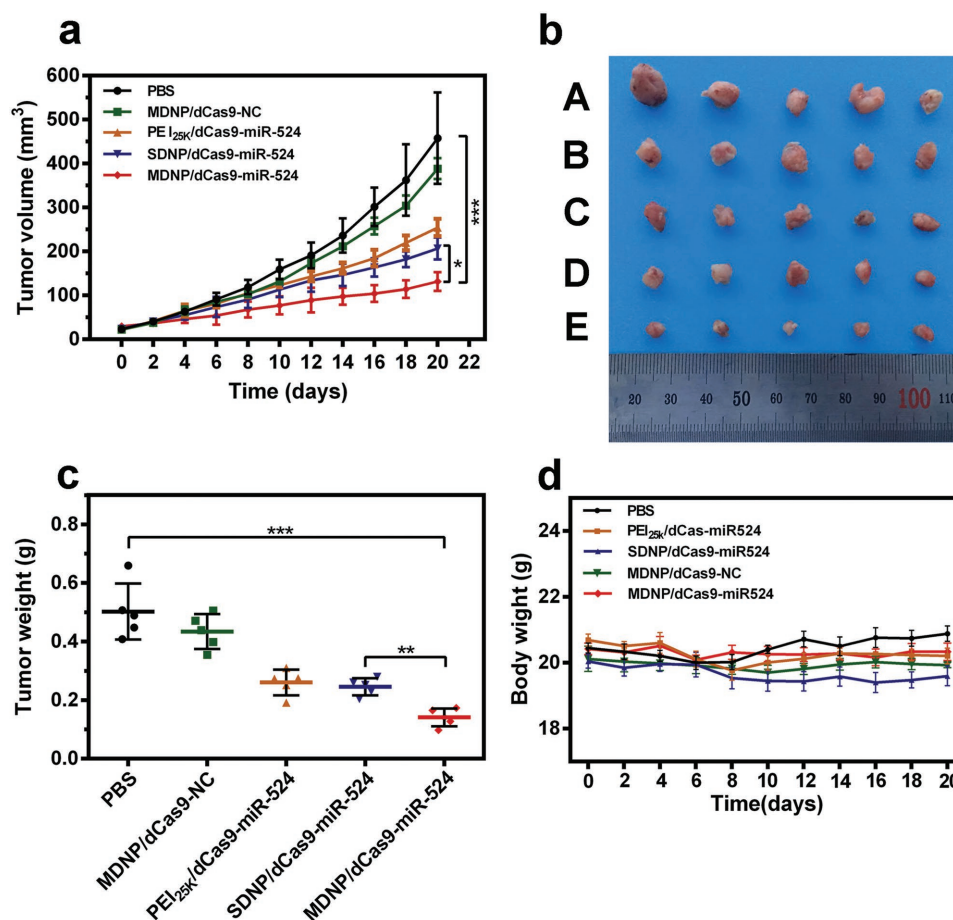


Figure 5. a) Tumor growth curves of the mice injected with PBS, MDNP/NC, PEI_{25k}/dCas9–miR-524, SDNP/dCas9–miR-524, MDNP/dCas9–miR-524, respectively. b) Ex vivo observation of the tumors from the treated mice 20 days postinjection (A: PBS, B: MDNP/NC, C: PEI_{25k}/dCas9–miR-524, D: SDNP/dCas9–miR-524, E: MDNP/dCas9–miR-524). c) Comparison of the weight of the tumors from the mice after treatment. d) Changes in body weight after treating the mice with different formulations. All data in (a), (b), (c), and (d) are presented as mean ± s.d. from five independent experiments (*n* = 5). The significant levels are shown as * *p* < 0.05, ** *p* < 0.01, and *** *p* < 0.001.

the tumors from the mice receiving MDNP/dCas9-miR-524 grew significantly slower than those with other treatments. This result was further confirmed by the ex vivo observation of the tumors (Figure 5b) and the comparison of the tumor weights (Figure 5c). Moreover, negligible variations of body weights were observed from the mice treated with MDNP (Figure 5d), suggesting the good biocompatibility of MDNP. Additionally, no elevation in inflammatory cytokine and immune globulin (Ig) secretion was observed from the mice treated with MDNP after the administration (Figures S14 and S15, Supporting Information), suggesting the low immunogenicity of MDNP. Further studies on the tumor tissues with RNA in situ hybridization (RISH) and immunohistochemistry (IHC) analyses confirmed that the tumor growth inhibition was associated with the CRISPR/dCas9-miR-524-mediated gene transcription regulation. According to the RISH and IHC analyses, the tumor from the MDNP/dCas9-miR-524-treated mice exhibited remarkably higher miR-524 expression level (Figure 6a), which led to significant inhibition of the expression of Smad2, Hes1, and Tead1 (Figure 6b). By inhibiting the essential proteins for TGF- β , Norch, and Hippo signaling pathways, MDNP/dCas9-miR-524

effectively triggered the apoptosis of the tumor cells,^[21,22] which was confirmed by the direct observation of the slices stained with hematoxylin and eosin (H&E) and terminal deoxynucleotidyl transferase 2'-deoxyuridine 5'-triphosphate (dUTP) nick end labeling (TUNEL) (Figure 6c,d), respectively. The effective inhibition of tumor growth confirmed the feasibility of applying CRISPR/dCas9-miR-524 system in vivo for cancer treatment with the aid of a properly designed delivery system. Furthermore, the relative expressions of Pri-miR-524 levels in tumors and normal organs were analyzed by qRT-PCR. As shown in Figure 6e, the tumors from the mice treated with MDNP/dCas9-miR-524 exhibited significantly elevated Pri-miR-524 levels (2.92-fold higher than those from the mice treated with PBS), suggesting the successful upregulation by MDNP/dCas9-miR-524. More importantly, upregulation of Pri-miR-524 was not observed from the nontargeted organs (e.g., heart, liver, spleen, lung, and kidney) of the mice treated with MDNP/dCas9-miR-524 (Figure 6f), suggesting the reduced off-target effects that may cause potential side effects. Considering the presence of the target gene of dCas9-miR-524 in both the tumors and these nontargeting organs, such tumor targeting performance has to be attributed to the tumor-targeting

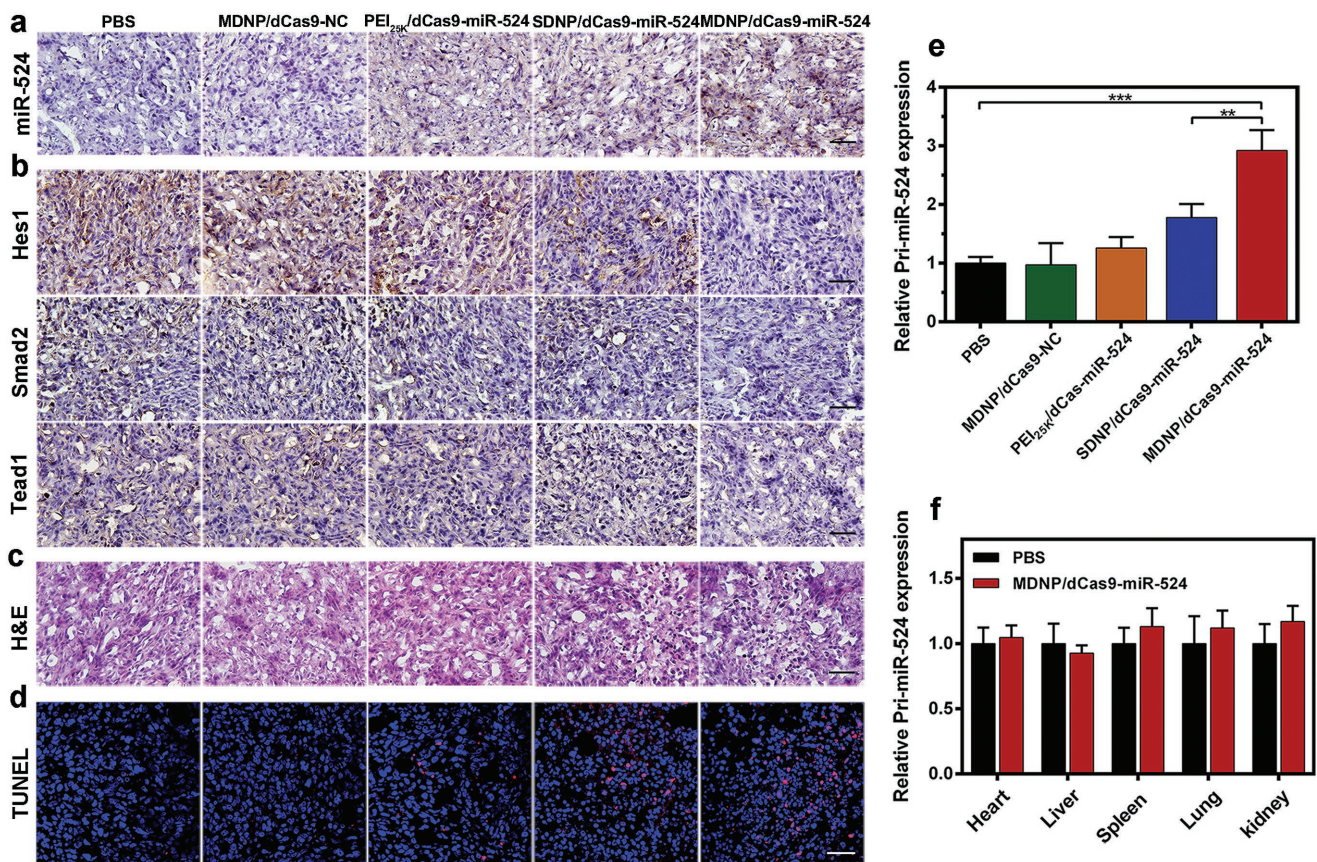


Figure 6. a) RNA in situ hybridization presenting the expression level of miR-524 in the tumor tissue from the mice in each treatment group. Cell nuclei are stained blue, and miR-524 are stained brown. The scale bar is 100 μ m. b) Immunohistochemistry analyses of the expression of Hes1, Tead1, and Smad2 in each treatment group, nuclei are stained blue, and the proteins are stained brown. The scale bar is 100 μ m. c,d) H&E staining (c) and TUNEL (d) analysis of the tumor tissues from the mice in each treatment group. The scale bar is 100 μ m. In TUNEL staining, normal cell nuclei are stained blue and apoptotic cell nuclei are stained red. The scale bar is 100 μ m. e,f) Relative expression levels of Pri-miR-524 in tumors (e) and nontargeted organs (f) from the mice treated with MDNP/dCas9-miR-524 and PBS, respectively. All data in (e) and (f) are presented as mean \pm s.d. from five independent experiments ($n = 5$). The significant levels are shown as ** $p < 0.01$ and *** $p < 0.001$.

capability of MDNP as well as the responsive release of dCas9–miR-524 from MDNP stimulated by the acidic tumor microenvironment. With the remarkable antitumor effect, reduced off-target effect, and low immunogenicity, MDNP/dCas9–miR-524 presented its potential in the development of novel CRISPR/dCas9-based cancer gene therapies.

3. Discussion

CRISPR/dCas9 system is one of the most powerful tools for the precise and efficient control of endogenous gene expression.^[2] Unlike CRISPR/Cas9 systems that require cutting and mutating the genome, CRISPR/dCas9 regulates the endogenous gene expression at transcription level.^[2] Since tumor growth can be relieved by suppressing oncogenes or upregulating tumor suppressor genes,^[6] CRISPR/dCas9 holds great potential for the development of safe and effective anticancer therapeutics.^[4] However, lack of efficient delivery systems, especially for the *in vivo* tumor-targeted delivery systems, prevents its clinical translation. For a successful CRISPR/dCas9-based cancer treatment *in vivo*, it is required for a delivery system to meet several design criteria including 1) a negatively charged and antiprotein-fouling surface to evade the blood clearance during circulation, and 2) a positively charged and membrane-binding surface to facilitate the intracellular transport of CRISPR/dCas9 system to allow it to function normally.^[12] However, those requirements seem conflicting with each other, preventing the construction of an ideal delivery system for CRISPR/dCas9 systems.

After a careful analysis of the delivery route, we realized that a tumor-targeted delivery of CRISPR/dCas9 had to experience three delivery stages, including circulating in blood after the administration (Stage 1), reaching and accumulating in tumor tissues (Stage 2), internalizing into tumor cells (Stage 3). The markedly different microenvironments between blood circulation and tumor tissues offer us the opportunity to simultaneously achieve all the desired features with one delivery system to overcome all the major delivery barriers of CRISPR/dCas9 systems. In this report, we present a MDNP which displays different surface properties in response to the change of the surrounding microenvironment. To achieve this feature, the MDNP is designed as a core–shell structure, in which the core is a PBA-modified cationic polyplex and the shell is made of a PEG-based responsive polymer (Figure 1a). By administration and circulation in blood (Stage 1), MDNP maintains a stable core–shell structure with a negatively charged and PEGylated surface, which is arguably the most practical method to enhance the circulation stability of nanoparticles. Due to the EPR effects, MDNP enters tumor tissues eventually (Stage 2). The acidic tumor microenvironment triggers the dissociation of the polymer shell from the MDNP, leading to the exposure of the cationic polyplex. Since the cationic surface has a much stronger electrostatic attraction to tumor tissues, the polyplex will stay and accumulate in tumor tissues. Moreover, the polyplex was modified with PBA groups, which bind to the sialic acids that are usually overexpressed by cancer cells and enhance the intracellular uptake of the polyplex (Stage 3). With this design, MDNP can present different surface properties in

the different delivery stages, which fulfills all the requirements simultaneously for achieving an efficient delivery of CRISPR/dCas9 system.

The delivery efficiency of MDNP was evaluated both *in vitro* and *in vivo* using fluorescence-labeled pDNA as a model. A significant enhancement in cellular uptake of the pDNA was observed when delivering with MDNP in acidic condition (pH 6.5) compared to the uptake in neutral condition (pH 7.4) (Figure 2g,j). This result confirms the acid-triggered dissociation of the MDNP shell, indicating that MDNP is capable to evade the cellular uptake under neutral pH (e.g., in blood), while internalizes into cells effectively under acidic pH (e.g., in tumor tissues). In mice, biodistribution analysis confirmed this result, indicating a significantly higher tumor-targeting efficiency of MDNP than other delivery carriers (Figure 4a,b). Less liver accumulation was also observed when delivering pDNA with MDNP compared to that delivered with PEI_{25k}, suggesting the effective immune clearance evasion due to PEGylated surface. Moreover, MDNP also exhibited faster and more efficient tumor targeting compared to SDNP, indicating that the dissociation of the PEGylated shell of MDNP and the exposure of the cationic polyplex in response to the acidic tumor microenvironment did enhance the tumor accumulation, which eventually increase the uptake of the pDNA by cancer cells (Figure 4c).

As a delivery system specially designed for CRISPR/dCas9-based cancer gene therapy, the performance of CRISPR/dCas9-based gene expressing regulation and antitumor effects were investigated both in cell and in mice. In these studies, we employed dCas9–miR-524 as the CRISPR/dCas9 system since the successful delivery of dCas9–miR-524 could activate the expression of miR-524, which then inhibited the expressions of three essential proteins related to cancer cell proliferation. Consistent with the delivery efficiency studies, increased expression level of miR-524 was observed in the cells treated with MDNP/dCas9–miR-524 in acidic condition (Figure 3b,c), and the eventual downregulation of Smad2, Hes1, and Tead1 (Figure 3d,e) led to the significant loss in cell viability when incubating cancer cells with MDNP (Figure 3f,g). Administration of MDNP/dCas9–miR-524 to tumor-bearing mice resulted in a remarkable inhibition in tumor growth (Figure 5a–c), which was caused by the activation of miR-524 expression that led to the apoptosis of tumor cells (Figure 6c,d). These results confirmed the successful *in vivo* CRISPR/dCas9-based gene expressing regulation achieved using MDNP, suggesting the potential of MDNP/dCas9–miR-524 as an effective strategy for the development of CRISPR/dCas9-based cancer gene therapy.

4. Conclusion

In conclusion, we have demonstrated a multistage delivery nanoparticle that can deliver CRISPR/dCas9 systems and facilitate effective regulation on gene expression both *in vitro* and *in vivo*. Systemic administration of MDNP/dCas9–miR-524 to tumor-bearing mice presented remarkable effects on tumor growth inhibition, suggesting the feasibility to utilize MDNP to achieve tumor-targeting delivery of CRISPR/dCas9

with sufficient level to realize its therapeutic effects. More importantly, the microenvironment-responsive polymer shell endows MDNP with the capability to present different surface properties at different delivery stages, allowing the MDNP to overcome multiple physiological barriers and deliver the payload to tumor tissues with an optimal efficiency. With these capabilities, MDNP could become a fundamental technology to address the delivery problems in the development of CRISPR/dCas9-based cancer gene therapy. More broadly, MDNP could be also adapted to deliver other types of CRISPR systems to raise exciting opportunities for novel CRISPR-based cancer treatments.

5. Experimental Section

Synthesis of PEI–PBA: The synthesis of PEI–PBA was achieved by conjugating 2-bromomethylphenylboronic acid onto branched PEI. Briefly, 1.80 g of PEI ($M_w = 1.8$ kDa) was first dissolved in methanol to reach a concentration of 120 mg mL⁻¹, and then 0.54 g of 2-bromomethylphenylboronic acid was added. The reaction solution was stirred under reflux at 70 °C for 12 h, and then the product was precipitated by dropping the reaction solution into cold ether. The successful conjugation was confirmed using ¹H NMR analysis, indicating that the molecular weight of the PEI–PBA was 2068 Da. Detailed synthesis procedures and characterizations are provided in the Supporting Information.

Synthesis of mPEG₁₁₃-b-PLys₁₀₀/DMMA and mPEG₁₁₃-b-PLys₁₀₀/SA: The synthesis of mPEG₁₁₃-b-PLys₁₀₀/DMMA was achieved by conjugating DMMA onto mPEG₁₁₃-b-PLys₁₀₀ (detailed synthesis procedures and characterizations are provided in the Supporting Information) Briefly, 100 mg of mPEG₁₁₃-b-PLys₁₀₀ was dissolved in sodium bicarbonate buffer (pH 8.5, 50 × 10⁻³ M) to reach a concentration of 10 mg mL⁻¹, and then 211.2 mg of DMMA (five equivalents to the amino groups of mPEG₁₁₃-b-PLys₁₀₀) was added. After the action, unreacted DMMA was removed by dialysis, and mPEG₁₁₃-b-PLys₁₀₀/DMMA was obtained by lyophilization. The synthesis of mPEG₁₁₃-b-PLys₁₀₀/SA was similar to that of mPEG₁₁₃-b-PLys₁₀₀/DMMA by replacing DMMA with SA. The successful synthesis was confirmed using ¹H NMR analysis that ≈90% of the amine groups on mPEG₁₁₃-b-PLys₁₀₀ reacted with DMMA or SA. Detailed synthesis procedures and characterizations are provided in the Supporting Information.

Preparation of MDNP and SDNP: The MDNP and SDNP were prepared by mixing mPEG₁₁₃-b-PLys₁₀₀/DMMA and mPEG₁₁₃-b-PLys₁₀₀/SA solutions with the solution of PEI–PBA/pDNA polyplex, respectively. First, the PEI–PBA (0.1 mL, 1.5 mg mL⁻¹ in water) and dCas9–miR-524 pDNA (0.1 mL, 250 μg mL⁻¹ in water) were mixed gently and incubated for 15 min to form the PEI–PBA/pDNA polyplex. Then, the mPEG₁₁₃-b-PLys₁₀₀/DMMA (0.1 mL, 3 mg mL⁻¹) and mPEG₁₁₃-b-PLys₁₀₀/SA (0.1 mL, 3 mg mL⁻¹) were added to the solution of PEI–PBA/pDNA polyplex (0.1 mL) and incubated for another 15 min to form MDNP and SDNP, respectively.

In Vitro CRISPR Activation of miR-524 Expression with MDNP in Cancer Cells: qRT-PCR and Western blot were performed to study in vitro CRISPR activation of miR-524 expression with MDNP in cancer cells. Briefly, MDA-MB-231 and LN-229 cells were seeded into 6-well plates at a density of 2 × 10⁵ cells per well and incubated overnight in 2 mL Dulbecco's modified Eagle medium (DMEM) with 10% FBS v/v. Before the transfection, the culture medium was replaced with the fresh ones and adjusted to pHs 7.4 and 6.8, respectively, following by the addition of 100 μL of MDNP solution (3 μg dCas9–miR-524 pDNA per well). After 4 h incubation, the culture medium was removed, and the cells were cultured with 2 mL fresh medium for further 48 h. The RNA and the proteins were extracted for qRT-PCR and Western blot analysis. More detailed procedures are provided in the Supporting Information.

In Vitro Cytotoxicity Analysis: The in vitro antitumor effect was studied by evaluate the viability of the cancer cells (MDA-MB-231 and LN-229) after treating with MDNP/dCas9–miR-524 at pH 7.4 and pH 6.5. Briefly, cells were seeded into 96-well plates at a density of 5 × 10³ cells per well and incubated overnight in 100 μL DMEM with 10% FBS v/v. Before transfection, the culture medium was replaced with 100 μL fresh ones and adjusted to pHs 7.4 and 6.8, respectively. 10 μL of the MDNP was added into the cell cultures to reach 200 ng pDNA per well. After 4 h incubation, the culture medium was removed, and the cells were cultured in fresh medium for another 24, 48, and 72 h, respectively. For the comparison, PEI_{25k}/pDNA polyplex and MDNP/NC were employed to perform the same studies. After the treatment, cell viability was assessed using CCK-8 assay. The cell viability was calculated by referring to the control group without any treatment.

In Vivo Distribution and Imaging: The tumor-bearing mice were generated by subcutaneous injection of MDA-MB-231 cells (5 × 10⁶ for each mouse) in the mammary fat pad, and the mice were randomly divided into three groups. When the tumor volume was about 400 mm³, three groups of the mice were intravenously injected with 100 μL of PEI_{25k}/pDNA polyplex, SDNP, and MDNP, all of which contained 10 μg TOTO-3-labeled pDNA, respectively. The distribution of the pDNA was imaged using IVIS Lumina imaging system (Caliper Life Sciences, USA) at 1, 6, and 24 h postinjection. The results were analyzed using Living Image 3.1 software (Caliper Life Sciences). To determine the distribution of TOTO-3-labeled pDNA in tumor, the tumor tissues were fixed, and the tissue sections were observed using a CLSM (Olympus, FV1000). More detailed procedures are provided in the Supporting Information.

In Vivo Tumor Inhibition: The tumor-bearing mice were established as described above. When the tumor volume was around 25 mm³ at 10 days after the cell implantation, the mice were randomly divided into five groups (five mice per group) and intravenously injected with 100 μL of PBS, MDNP/dCas9–NC, PEI_{25k}/dCas9–miR-524, SDNP/dCas9–miR-524, and MDNP/dCas9–miR-524 containing 10 μg pDNA per mouse every 3 days, respectively. Tumor growth was monitored by measuring the perpendicular diameter of the tumor using calipers. The estimated volume was calculated according to the formula: tumor volume (mm³) = 0.5 × length × width². After finishing the treatment, the tumors were harvested from the mice. The expression of miR-524 in tumor tissues was detected by qRT-PCR and RISH. IHC was performed for analyzing the expression levels of Hes1, Tead1, and Smad2. For the observation of tumor cell apoptosis, tumor slices were stained with H&E and TUNEL, respectively. All the images were recorded using CLSM (Olympus, FV1000) or a fluorescence microscope (Olympus, CX41). More detailed procedures are provided in the Supporting Information.

Supporting Information

Supporting Information is available from the Wiley Online Library or from the author.

Acknowledgements

Q.L. and K.Z. contributed equally to this work. This work was supported by grants from the National Key Research and Development Programs of China (Grant Nos. 2018YFA0209700 and 2016YFC0902502), the National Natural Science Foundation of China (NSFC, Grant Nos. 51673100, 91527306, 51503122, 81602208 and PCSIRT (Grant No. IRT1257)), the Thousand Talents Program for Young Professionals, and the Fundamental Research Funds for the Central Universities.

Conflict of Interest

The authors declare no conflict of interest.

Keywords

cancer therapy, CRISPR/dCas9, gene regulation, miR-524, multistage delivery

Received: August 24, 2018

Revised: September 19, 2018

Published online: October 25, 2018

- [1] a) F. A. Ran, P. D. Hsu, C. Y. Lin, J. S. Gootenberg, S. Konermann, *Cell* **2013**, 154, 1380; b) F. A. Ran, P. D. Hsu, J. Wright, V. Agarwala, D. A. Scott, F. Zhang, *Nat. Protoc.* **2013**, 8, 2281.
- [2] a) L. A. Gilbert, M. A. Horlbeck, B. Adamson, J. E. Villalta, Y. Chen, E. H. Whitehead, C. Guimaraes, B. Panning, H. L. Ploegh, M. C. Bassik, L. S. Qi, M. Kampmann, J. S. Weissman, *Cell* **2014**, 159, 647; b) D. Bikard, W. Jiang, P. Samai, A. Hochschild, F. Zhang, L. A. Marraffini, *Nucleic Acids Res.* **2013**, 41, 7429; c) S. Konermann, M. D. Brigham, A. E. Trevino, J. Joung, O. O. Abudayyeh, C. Barcena, P. D. Hsu, N. Habib, J. S. Gootenberg, H. Nishimasu, O. Nureki, F. Zhang, *Nature* **2015**, 517, 583.
- [3] a) D. Hanahan, R. A. Weinberg, *Cell* **2000**, 100, 57; b) D. Hanahan, R. A. Weinberg, *Cell* **2011**, 144, 646.
- [4] F. J. Sanchez-Rivera, T. Jacks, *Nat. Rev. Cancer* **2015**, 15, 387.
- [5] M. Renteln, *Gene Ther.* **2018**, 25, 1.
- [6] I. B. Hilton, A. M. D'Ippolito, C. M. Vockley, P. I. Thakore, G. E. Crawford, T. E. Reddy, C. A. Gersbach, *Nat. Biotechnol.* **2015**, 33, 510.
- [7] J. Joung, S. Konermann, J. S. Gootenberg, O. O. Abudayyeh, R. J. Platt, M. D. Brigham, N. E. Sanjana, F. Zhang, *Nat. Protoc.* **2017**, 12, 828.
- [8] J. C. Nault, S. Datta, S. Imbeaud, A. Franconi, M. Mallet, G. Couchy, E. Letouze, C. Pilati, B. Verret, J. F. Blanc, C. Balabaud, J. Calderaro, A. Laurent, M. Letexier, P. Bioulac-Sage, F. Calvo, J. Zucman-Rossi, *Nat. Genet.* **2015**, 47, 1187.
- [9] H. Yin, R. L. Kanasty, A. A. Eltoukhy, A. J. Vegas, J. R. Dorkin, D. G. Anderson, *Nat. Rev. Genet.* **2014**, 15, 541.
- [10] a) M. Wang, J. A. Zuris, F. Meng, H. Rees, S. Sun, P. Deng, Y. Han, X. Gao, D. Pouli, Q. Wu, I. Georgakoudi, D. R. Liu, Q. Xu, *Proc. Natl. Acad. Sci. USA* **2016**, 113, 2868; b) H. Yin, C.-Q. Song, J. R. Dorkin, L. J. Zhu, Y. Li, Q. Wu, A. Park, J. Yang, S. Suresh, A. Bizhanova, A. Gupta, M. F. Bolukbasi, S. Walsh, R. L. Bogorad, G. Gao, Z. Weng, Y. Dong, V. Koteliensky, S. A. Wolfe, R. Langer, W. Xue, D. G. Anderson, *Nat. Biotechnol.* **2016**, 34, 328; c) J. B. Miller, S. Zhang, P. Kos, H. Xiong, K. Zhou, S. S. Perelman, H. Zhu, D. J. Siegwart, *Angew. Chem., Int. Ed.* **2017**, 56, 1059.
- [11] a) R. Mout, M. Ray, G. Y. Tonga, Y. W. Lee, T. Tay, K. Sasaki, V. M. Rotello, *ACS Nano* **2017**, 11, 2452; b) P. Wang, L. Zhang, W. Zheng, L. Cong, Z. Guo, Y. Xie, L. Wang, R. Tang, Q. Feng, Y. Hamada, K. Gonda, Z. Hu, X. Wu, X. Jiang, *Angew. Chem., Int. Ed.* **2018**, 57, 1491; c) K. Lee, M. Conboy, H. M. Park, F. Jiang, H. J. Kim, M. A. Dewitt, V. A. Mackley, K. Chang, A. Rao, C. Skinner, T. Shobha, M. Mehdipour, H. Liu, W. C. Huang, F. Lan, N. L. Bray, S. Li, J. E. Corn, K. Kataoka, J. A. Doudna, I. Conboy, N. Murthy, *Nat. Biomed. Eng.* **2017**, 1, 889.
- [12] a) J. Sun, C. Luo, Y. Wang, Z. He, *Nanoscale* **2013**, 5, 845; b) S. Eteezadi, S. N. Ekdawi, C. Allen, *Adv. Drug Delivery Rev.* **2015**, 91, 7.
- [13] a) S. E. A. Gratton, P. A. Ropp, P. D. Pohlhaus, J. C. Luft, V. J. Madden, M. E. Napier, J. M. DeSimone, *Proc. Natl. Acad. Sci. USA* **2008**, 105, 11613; b) K. Knop, R. Hoogenboom, D. Fischer, U. S. Schubert, *Angew. Chem., Int. Ed.* **2010**, 49, 6288; c) Y. Lee, K. Miyata, M. Oba, T. Ishii, S. Fukushima, M. Han, H. Koyama, N. Nishiyama, K. Kataoka, *Angew. Chem., Int. Ed.* **2008**, 47, 5163.
- [14] J. Z. Du, C. Q. Mao, Y. Y. Yuan, X. Z. Yang, J. Wang, *Biotechnol. Adv.* **2014**, 32, 789.
- [15] M. A. Mintzer, E. E. Simanek, *Chem. Rev.* **2009**, 109, 259.
- [16] a) S. Deshayes, H. Cabral, T. Ishii, Y. Miura, S. Kobayashi, T. Yamashita, A. Matsumoto, Y. Miyahara, N. Nishiyama, K. Kataoka, *J. Am. Chem. Soc.* **2013**, 135, 15501; b) K. Djanashvili, L. Frullano, J. A. Peters, *Chem. - Eur. J.* **2005**, 11, 4010; c) A. Matsumoto, H. Cabral, N. Sato, K. Kataoka, Y. Miyahara, *Angew. Chem., Int. Ed.* **2010**, 49, 5494.
- [17] a) Y. Lee, K. Miyata, M. Oba, T. Ishii, S. Fukushima, M. Han, H. Koyama, N. Nishiyama, K. Kataoka, *Angew. Chem., Int. Ed.* **2008**, 120, 5241; b) A. Akinc, M. Thomas, A. M. Klibanov, R. Langer, *J. Gene Med.* **2005**, 7, 657.
- [18] a) D. Fischer, Y. X. Li, B. Ahlemeyer, J. Kriegelstein, T. Kissel, *Biomaterials* **2003**, 24, 1121; b) E. Jin, B. Zhang, X. Sun, Z. Zhou, X. Ma, Q. Sun, J. Tang, Y. Shen, E. V. Kirck, W. J. Murdoch, M. Radosz, *J. Am. Chem. Soc.* **2013**, 135, 933.
- [19] S. Li, Q. Zou, Y. Li, C. Yuan, R. Xing, X. Yan, *J. Am. Chem. Soc.* **2018**, 140, 10794.
- [20] a) K. Remaut, N. N. Sanders, B. G. De-Geest, K. Braeckmans, J. Demeester, S. C. De-Smedt, *Mater. Sci. Eng., R* **2007**, 58, 117; b) D. W. Pack, A. S. Hoffman, S. Pun, P. S. Stayton, *Nat. Rev. Drug Discovery* **2005**, 4, 581.
- [21] K. Zhao, Q. Wang, Y. Wang, K. Huang, C. Yang, Y. Li, K. Yi, C. Kang, *Cancer Lett.* **2017**, 406, 12.
- [22] a) K. Seystahl, I. Tritschler, E. Szabo, G. Tabatabai, M. Weller, *Neuro-Oncology* **2015**, 17, 254; b) K. C. Schreck, P. Taylor, L. Marchionni, V. Gopalakrishnan, E. E. Bar, N. Gaiano, C. G. Eberhart, *Clin. Cancer Res.* **2010**, 16, 6060; c) A. M. Tremblay, E. Misasiaglia, G. G. Galli, S. Hettmer, R. Urcia, M. Carrara, R. N. Judson, K. Thway, G. Nadal, J. L. Selfe, G. Murray, R. A. Calogero, C. De-Bari, P. S. Zammit, M. Delorenzi, A. J. Wagers, J. Shipley, H. Wackerhage, F. D. Camargo, *Cancer Cell* **2014**, 26, 273.
- [23] a) U. Prabhakar, H. Maeda, R. K. Jain, E. M. Sevick-Muraca, W. Zamboni, O. C. Farokhzad, S. T. Barry, A. Gabizon, P. Grodzinski, D. C. Blakey, *Cancer Res.* **2013**, 73, 2412; b) J. Wang, W. Mao, L. L. Lock, J. Tang, M. Sui, W. Sun, H. Cui, D. Xu, Y. Shen, ACS Nano **2015**, 9, 7195; c) L. K. Bogart, G. Pourroy, C. J. Murphy, V. Puentes, T. Pellegrino, D. Rosenblum, D. Peer, R. Levy, *ACS Nano* **2014**, 8, 3107.